CHARACTERIZING MODE I STRAIN ENERGY RELEASE RATE ASSOCIATED WITH INTERFACIAL DEBOND GROWTH IN SANDWICH COMPOSITES

by

Joseph O. Nelson

A thesis submitted to the faculty of
The University of Utah
in partial fulfillment of the requirements for the degree of

Master of Science

Department of Mechanical Engineering

The University of Utah

December 2012

The University of Utah Graduate School

STATEMENT OF THESIS APPROVAL

The thesis of **Joseph O. Nelson**

has been approved by the following supervisory committee members:

Daniel Adams	, Chair	**11/16/2012** Date Approved
K. Larry DeVries	, Member	**11/16/2012** Date Approved
Ken Monson	, Member	**11/16/2012** Date Approved

and by **Timothy Ameel**, Chair of the Department of **Mechanical Engineering**

and by Charles A. Wight, Dean of The Graduate School.

ABSTRACT

This work is aimed towards the development of a standardized test to quantify the critical strain energy release rate, G_c, of debond growth along the facesheet/core interface under Mode I loading of sandwich composites. The single cantilever beam (SCB) configuration is used throughout this research and was seen to consistently propagate debonds along the facesheet/core interface for a wide variety of sandwich constructions, including both foam and honeycomb cores. A test fixture is described which utilizes an edgewise clamping base and lengthened loading rod to ensure Mode I dominated debond growth throughout the test. Specimen geometry and sizing (specifically specimen width, facesheet thickness, and initial debond location) are investigated in depth analytically using the Virtual Crack Closure Technique (VCCT) and experimentally using the Compliance Calibration (CC) method to ensure high (greater than 95%) Mode I dominance and accurate G_c measurements.

Anticlastic bending of facesheets and plane stress conditions along the edges of the specimen were seen to cause debond curvature. For sandwich composites with cores of a continuous bond surface, a specimen width of 50.8 mm (2 in.) was seen to be sufficient to achieve fully developed, self similar debond growth. For cores of a discontinuous bond surface, a minimum specimen width of 50.8 mm (2 in.) and at least 6 cells across the specimen width was seen to be sufficient to achieve consistent G_c measurements. Facesheet thickness was not seen to alter debond growth, except when tabbing was bonded to thin facesheeted constructions in an effort to reduce deflections.

The tabbed specimen saw a change in failure mode, which was also evident in G_c measurements. Initial debond location was not seen to be a factor in any of the testing. Debonds above, below, and in the interfacial bondline were all seen to propagate along the same path and debonds located at the centerline of the core were seen to "self-adjust" and shift from the centerline to the upper facesheet/core interface.

For Lissa

TABLE OF CONTENTS

LIST OF FIGURES

LIST OF TABLES

ACKNOWLEDGEMENTS

Completing a project of this breadth and depth would not have been possible without the guidance and help of a caring advisor. I would like to express my appreciation for Dr. Adams and thank him for giving me the opportunity to be involved in this research. I would not have been able to complete this work without the council and direction I received the many times I met with him to review my progress and discuss findings. He gave me the freedom to work at my own pace while challenging me to dig deeper into some of the more complex issues. The time I spent working with him will always be regarded as the highlight of my educational career, and I'll carry the knowledge I gained during this project for the remainder of my life.

In addition, I would like to thank Brad Kuramoto for the work he did preceding mine. He provided a solid foundation on which I was able to start my research. The advice and tips he gave me were greatly appreciated.

There are too many to name here, but I would also like to thank the other graduate students in the Composites Lab and for the friendships which were built as we worked and joked together.

Lastly, I would like to thank my wife, Lissa, for the love and support she showed as I completed my research. It certainly was a journey to get where I am today, and she was there supporting me every step along the way.

1 INTRODUCTION

Sandwich constructions consist of two thin composite facings that are bonded to a lower modulus core. The sandwich configuration creates a very stiff, lightweight structure and for this reason is often used in aerospace applications where increased stiffness, strength and weight minimization are critical. Similar to the web of an I-beam, which transmits shear forces between the two flanges, the core of a sandwich composite transmits shear forces between the two facings. Debonding of the facing(s) from the core affects stability and prevents load transfer between the core and facing, compromising the sandwich construction's strength. For this reason, maintaining the bond between the facings and the core is vital in allowing the sandwich construction to perform as it was designed.

The sandwich construction's ability to resist debond growth along the facing/core interface, or its interface fracture toughness, is dependent upon various factors. For example, cores with continuous bonding surfaces such as balsa wood or foam will have different strain energy release rates, G, than those constructions with discontinuous bonding surfaces, such as honeycomb. As well, a sandwich constructed of facings bonded to a core using a very brittle or weak adhesive will also have different G values than a sandwich made using a toughened adhesive. Therefore, even though two structures may be built using sandwich composites, their load carrying capability and their damage tolerance can be very different. For this reason, the ability to test a

sandwich construction and determine its critical strain energy release rate, $G_{c,}$ has increased in importance in recent years.

The American Society for Testing and Materials (ASTM) has standardized a Double Cantilever Beam (DCB) test for testing the Mode I interlaminar fracture toughness of composite laminates, ASTM Standard D 5528 [1]. Designed specifically for use on unidirectional laminates, this test has been adapted to be used on sandwich composites. One such adaptation has been the placement of the initial debond or precrack. Rather than the initial precrack being located at the center line of the specimen, as is the case when testing a laminate, the precrack location for sandwich composite DCB specimens has been repositioned to the facesheet/core interface, as seen in Figure 1-1. Testing sandwich coupons using the DCB test configuration, with the asymmetrically positioned debond, was found to cause specimen rotation. This rotation of the specimen caused debond growth to deviate from the interface into the core, a phenomenon referred to as crack kinking. Crack kinking was found to be an issue primarily with low density foam cores, however in all cases debond growth away from the interface was found to be undesirable when measuring the interface fracture toughness [2].

There are however, test standards which have been designed specifically to be used on sandwich composites or have been found to perform well with sandwich constructions. Flatwise Tension, ASTM C 297 [3] is one such test which was developed specifically to test the strength of the facesheet/core interface. However, flatwise tension testing reports the flatwise tensile strength of the core and the core-to-facing bond rather than the interface fracture toughness. Another test which is sometimes used in evaluating the interface fracture toughness of sandwich constructions is the Climbing Drum Peel

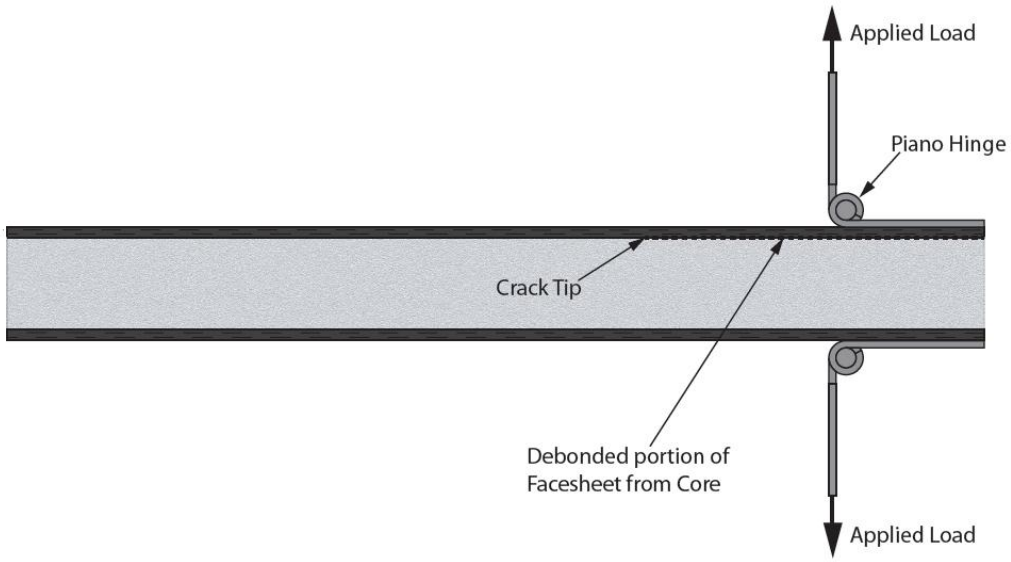

Figure 1-1: Double Cantilever Beam test configuration for sandwich composites

(CDP) test, ASTM D 1781 [4]. The issue with this test is that it yields a qualitative or comparative assessment of the bond rather than a fundamental measurement of the interface fracture toughness.

Recently, a research effort investigating alternative test methods specifically designed for quantitatively measuring the interface fracture toughness and G_c of sandwich composites has been undertaken at the University of Utah [5 and 6]. In this research many different test configurations were evaluated and compared to the DCB test method. Some of the key considerations in making these comparisons were maintaining debond growth along the facesheet/core interface without kinking into the core and high percentages of Mode I loading at the debond front. With test method standardization as the end goal, it was also necessary that the test method selected for standardization be suitable for a wide range of sandwich configurations. Some of the more promising candidates over the DCB method were found to be the Modified Double Cantilever

Beam, End Supported Single Cantilever Beam, Three-Point Flexure, and the Plate-Supported Single Cantilever Beam test configurations.

1.1 Modified Double Cantilever Beam (MDCB)

The Modified Double Cantilever Beam (MDCB) is similar to the DCB test configuration, however a support block is incorporated at the end of the specimen to prevent rotation, as seen in Figure 1-2. By decreasing specimen rotation it was hoped that crack kinking, which was present in DCB testing, would be decreased without affecting the high Mode I dominated loading condition which the DCB configuration produced. Coupon testing revealed however, that crack kinking was still an issue despite the additional specimen support the MDCB configuration provided. For this reason the MDCB configuration was not selected to be a suitable Mode I test method for sandwich composites [6].

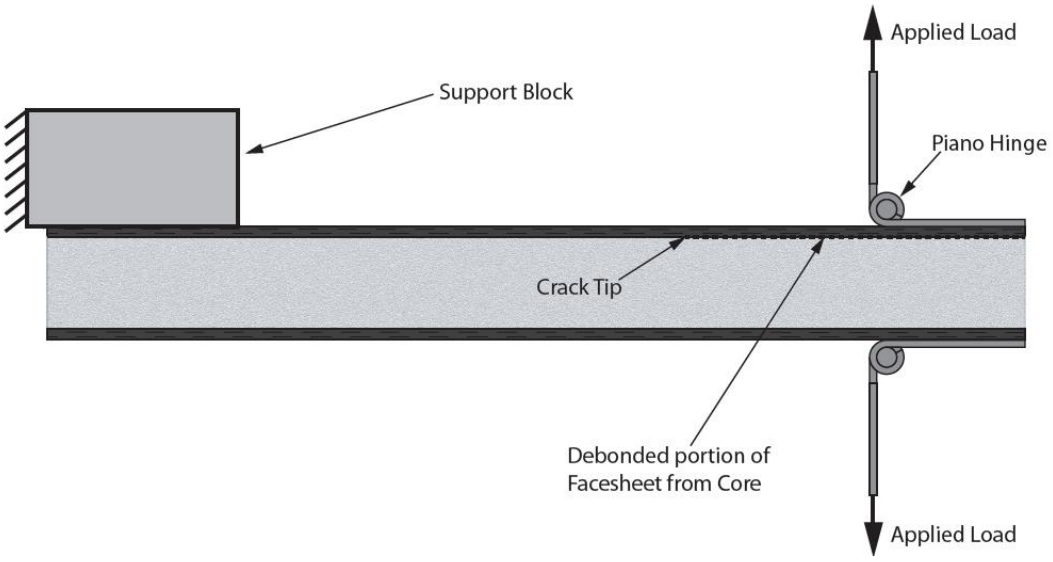

Figure 1-2: Modified Double Cantilever Beam test configuration

1.2 End Supported Single Cantilever Beam (ESSCB)

Another variation to the DCB test was the End Supported Single Cantilever Beam (ESSCB), as seen in Figure 1-3. Similarly to the manner the MDCB increased specimen support over the DCB, the ESSCB increased support over the MDCB specimen by adding a lower support block to the specimen. This additional support was added to reduce bending in the core and to minimize the Mode II component. However, despite the increased specimen support, testing concluded crack kinking still to be an issue with the ESSCB, and for this reason was not suggested for use in test method standardization [6].

1.3 Three-Point Flexure (TPF)

The Three-Point Flexure (TPF) test configuration shown in Figure 1-4, which varied significantly in means of load application and specimen support from the DCB, MDCB, or ESSCB configurations, was found to be successful in reducing crack kinking. However significant bending of the specimen led to increased shear stresses in the core

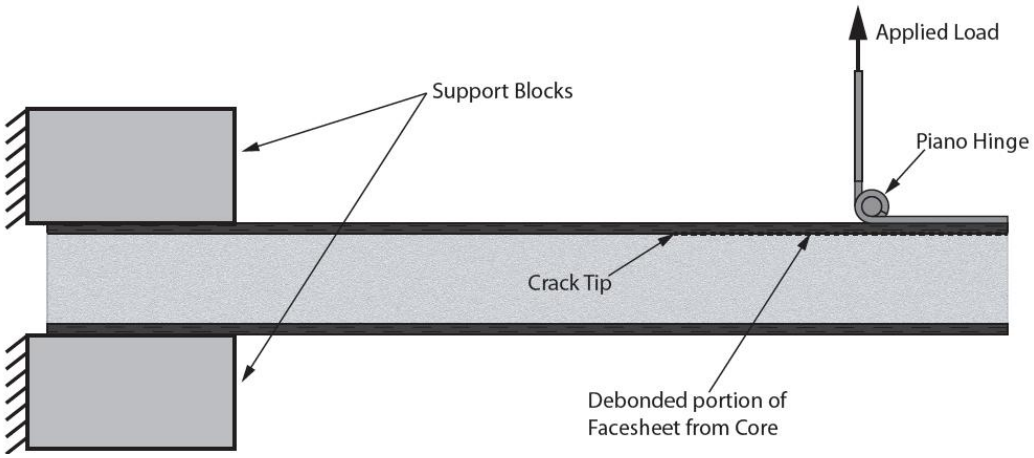

Figure 1-3: End Supported Single Cantilever Beam test configuration

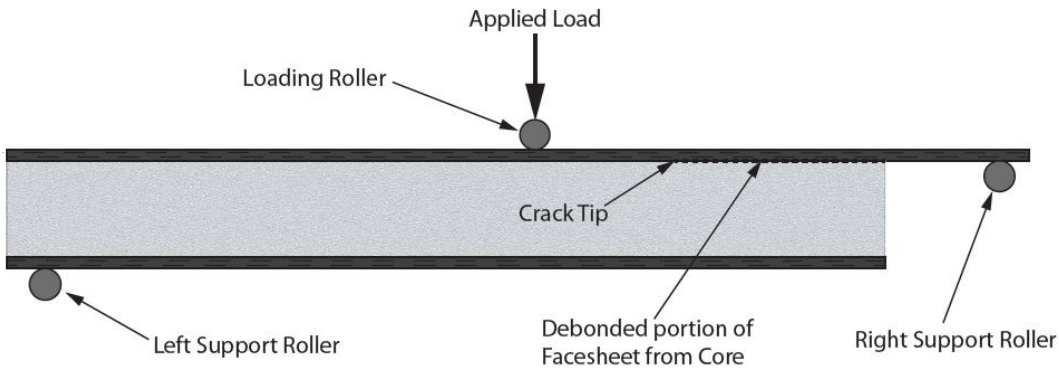

Figure 1-4: Three-Point Flexure test configuration

near the interface with the facesheet. As well, the level of involvement required for TPF specimen preparation was found to be undesirable. For these reasons the TPF was found not to be well suited for test standardization [6].

1.4 Plate-Supported Singe Cantilever Beam (SCB)

The Plate-Supported Single Cantilever Beam (SCB) configuration, shown in Figure 1-5, was also evaluated. This configuration, with the full base constraint of the specimen, eliminated the bending and rotating of the sandwich specimen and maintained high Mode I loading components. As well, crack kinking was not found to be present during any of the testing. Debond growth consistently occurred along the facesheet/core interface and the test fixturing accommodated a wide variety of sandwich sizes and configurations. For these reasons the SCB test configuration was selected as a suitable candidate for a standardized test method [6].

Based upon these initial findings, which showed the SCB test configuration to be the most suitable candidate for test method standardization, it is the focus of this research to further investigate the SCB test method and determine the fixturing and specimen geometry required for standardization. In addition to the geometric configuration of the

specimen, the effects that variations in the constituent material properties have on test results will be analyzed. It is hoped that this research will lead to the development of an ASTM standardized test method designed specifically for measuring G_c and determining the interface fracture toughness of various sandwich composites under Mode I loading.

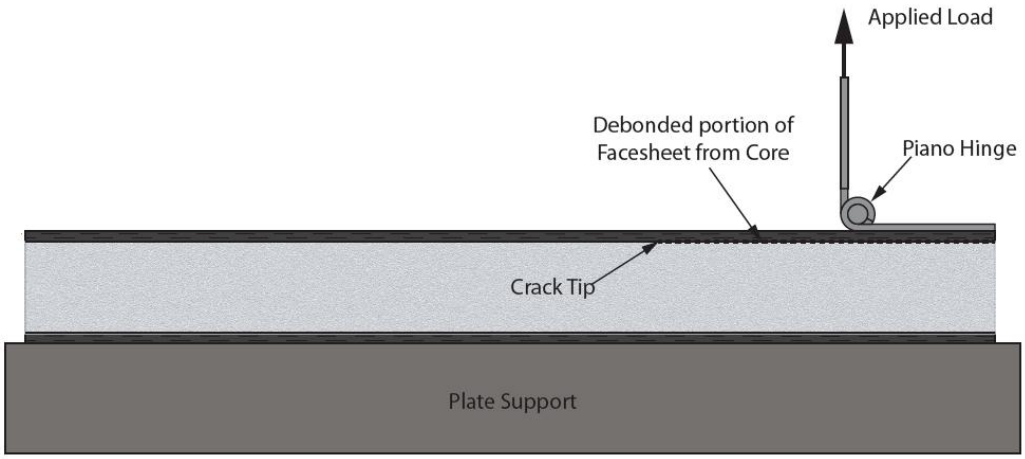

Figure 1-5: Single Cantilever Beam test configuration

2 MATERIALS

Throughout this research two different sandwich systems were investigated. Both constructions consisted of carbon/epoxy composite facings, however one utilized a foam core while the other was a honeycomb core. All fabrication took place at the University of Utah's Composite Mechanics Laboratory. The materials and fabrication techniques are described below.

2.1 Foam Core Sandwich Composite

The facesheets for the foam core sandwich panels were fabricated from Toray T300B 3K plane weave carbon fiber fabric. The core was a 12.7 mm (0.50 in.) thick 160 kg/m^3 (10 lb/ft^3) LAST-A-FOAM FR-6710 polyurethane foam core manufactured by General Plastics Manufacturing Co. The panels were fabricated using a Vacuum Assisted Resin Transfer Molding (VARTM) process, which is outlined in Appendix A. The resin used was a two-part epoxy consisting of EPON 862 resin and EPIKURE 9553 curing agent manufactured by Hexion Specialty Chemicals, now Momentive Specialty Chemicals Inc. The different facesheet configurations shown in Table 2-1 were selected for this project so as to evaluate effects resulting from variations in facesheet ply orientation.

Table 2-1. Foam core sandwich configurations of interest

Facesheet	Polyurethane Core [7]		
	Thickness (mm)	Density (kg/m^3)	Modulus (Mpa)
$[(0/90)_2]_S$	12.7	160	86
$[(0/90)/(\pm45)]_{3T}$	12.7	160	86

2.2 Honeycomb Core Sandwich Composite

The facesheets of the honeycomb core sandwich panels were constructed from either 5256-1 T300 12K 190/38-24 carbon fiber prepreg or Cycom 970/T300 12K prepreg, both of which were manufactured by Cytec Industries. Supply of the 5256-1 expired and it was not possible to procure additional material. For this reason a switch to the 970 prepreg was made for the remaining testing. Both prepregs are 350° F cure and have similar mechanical properties. For this study, the majority of the honeycomb core sandwich composites used a 3.18 mm (0.13 in.) cell size, 128 kg/m^3 (8.0 lb/ft^3) density Nomex honeycomb manufactured by Hexcel Corporation. A portion of testing was also conducted using specimen constructed from a honeycomb core of larger cell size and lighter density; 9.53 mm (0.38 in.) and 48 kg/m^3 (3.0 lb/ft^3), respectively. As well, one round of testing incorporated an aluminum honeycomb cored sandwich configuration which was provided to the University of Utah for testing.

The Nomex honeycomb sandwich panels were fabricated using a two-step process. First the facesheets were press-cured. They were then bonded to the Nomex core in a secondary bond procedure, as outlined in the Honeycomb Sandwich Manufacturing section of Appendix A. The majority of test specimens were manufactured using Hysol EA9689.10GK film adhesive manufactured by the Henkel Corporation. Similarly to the case of the carbon fiber prepreg, supply of the EA9689 ran

out and the remaining panels were fabricated using FM 300K 0.08 psf film adhesive, manufactured by Cytec. The FM 300 was used in place of the EA9698 film adhesive only for the honeycomb cell size testing described in Section 4.2.1.

During testing, facesheet thickness and cell size were varied in an attempt to evaluate their effects on G_c. In addition, G-10 fiberglass tabbing was added to thin facesheeted sandwich constructions to act as a doubler to verify whether very compliant facesheets could be artificially stiffened without adversely affecting G_c, as described in Section 5. Table 2-2 provides a complete list of the different honeycomb sandwich configurations used throughout testing.

Table 2-2. Honeycomb core sandwich configurations of interest

Facesheet	**Honeycomb Core** [8]			
	Thickness (mm)	**Density (kg/m3)**	**Cell Size (mm)**	**Material**
$[0/90/0]_S$	12.7	128	3	Nomex
		48	9	
$[0/90/0]_T$	12.7	128	3	Nomex
$[0/90/0]_T$ (.020" tabbing)				
$[0/90/0]_T$ (.0625" tabbing)				
$[(0/90/0)_2]_S$	12.7	128	3	Nomex
Quasi-isotropic	38.1	na	9	Aluminum

3 TEST FIXTURE

An important consideration in the development of this test method was the design of the test fixture. The fixture is required be sufficiently rigid and robust to support the coupon throughout the test. Yet, the fixture is also needed to be simple and versatile enough to handle a wide range of sandwich configurations and allow the test to be performed efficiently in a laboratory environment. Lastly, the fixture needed to allow for the measuring and gathering of data accurately without interfering with the natural failure of the specimen. A test fixture consisting of a simple yet effective base support and loading rod was developed and is explained hereafter.

3.1 Base Support

Supporting the specimen during testing could be as simple as permanently bonding the coupon to a loading plate; however this method of support, with the time required to bond and cure each specimen to the fixture between tests is unsuitable for laboratory use. Instead, an approach to secure the coupon to the base plate via an edgewise loading clamp was devised, illustrated in Figure 3-1. The horizontal edge clamps, which are bolted to the base plate via slotted holes, can be adjusted inward and outward to provide sufficient clamping force to hold the specimen securely to the base plate. To increase the clamping capability, the clamping surface of the edge clamps was beveled slightly inward. This method of support was found not only to secure the specimen, but it also acted to center the specimen on the fixture that aided in ensuring

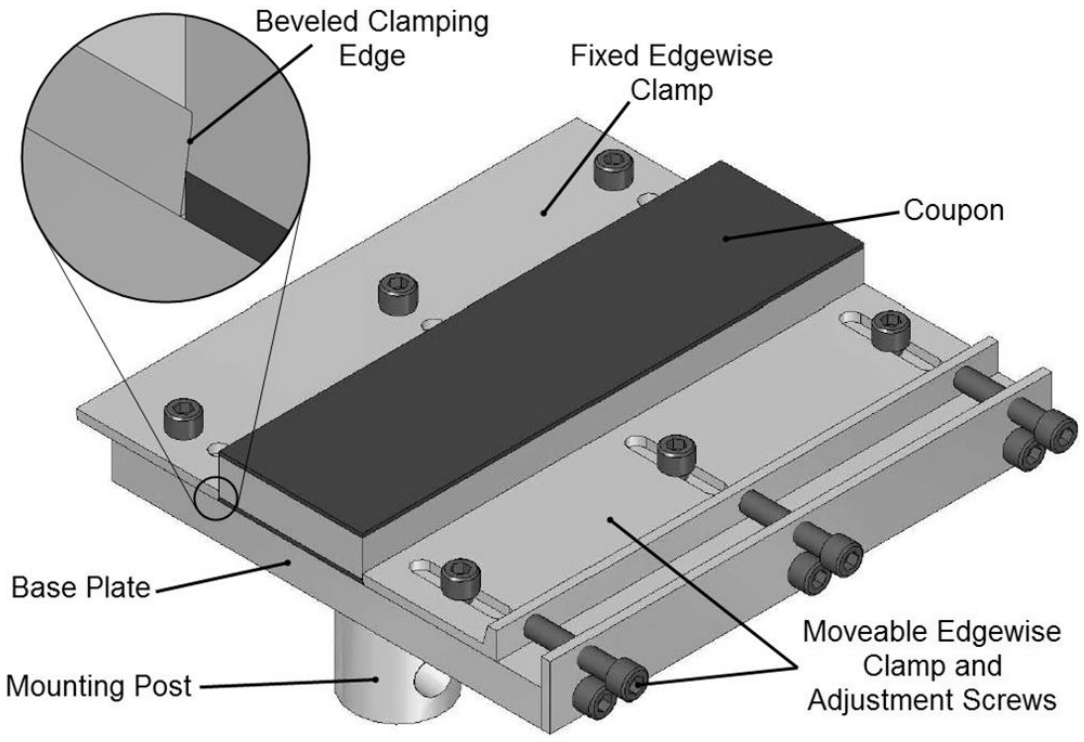

Figure 3-1: Test fixture and coupon showing edgewise clamping mechanism

proper loading. Using this edge constraining technique, it was found that test coupons could effectively be held during testing and quickly be changed out.

3.2 Load Application

To ensure that the loading at the debond front maintained a Mode I dominance throughout the test, it was necessary that the load path remained essentially vertical. To accomplish this, two methods were investigated. The first was to allow the base support to translate horizontally as the debond grew, in effect minimizing the Mode II loading components. The second method was to offset the load through the use of a lengthened loading rod, as was used by Li and Carlsson in their tilted sandwich debond (TSD) work [9].

Mode mixities for each of these two methods were investigated using finite element analysis (FEA) preformed in ANSYS v. 11.0, a finite element software package. A two-dimensional finite element model was constructed using PLANE42 elements; a four node element with two degrees of freedom at each node: translation in the nodal x and y directions. The FE model consisted of 1,680 square elements 1.27 mm (0.05 in.) in length. The facesheets were modeled as 1.27 mm (0.05 in.) thick by 178 mm (7.0 in.) in length. The core was the same length as the facesheets and its thickness was 12.7 mm (0.50 in.). Node merging was used to attach the facesheets to the core and node coupling was used to create the debond front. The finite element model is shown in Figure 3-2 and the material properties used during this analysis are shown in Table 3-1.

The first method for ensuring Mode I dominated debond growth (horizontal translation of the base support) was verified by constraining the lower facesheet in the FE model in only the y direction. This allowed the specimen to translate freely in the x direction. Analysis of the forces near the debond front showed increased Mode I loading when the specimen was allowed to translate in the x direction as compared to a fully constrained (x and y directions) specimen.

Based off of these findings and patterned after the FE model, a test fixture was designed and build which allowed horizontal translation of the specimen as shown in Figure 3-3. By increasing the degrees of freedom of the base plate and allowing

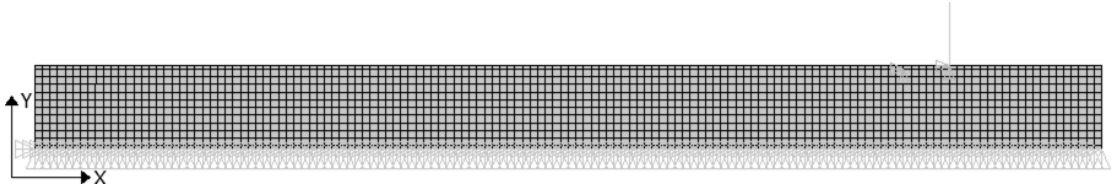

Figure 3-2: 2D Finite element model

Table 3-1: Mechanical Properties

Material	E_1 (GPa)	E_2 (GPa)	E_3 (GPa)	G_{12} (GPa)	G_{13} (GPa)	G_{32} (GPa)	ν_{12}	ν_{13}	ν_{32}
T300B 3K plain weave facesheet EPON 862 epoxy resin and EPON 953 hardener [10 and 11]	3.24E+01	3.24E+01	1.06E+01	3.86E+00	4.14E+00	4.14E+00	3.47E-01	2.60E-01	9.20E-02
Cytec 5256-1 T300 12K 190/38-24" unidirectional carbon fiber prepreg [10]	8.73E+01	4.79E+01	1.12E+01	5.86E+00	5.06E+00	4.26E+00	4.39E-02	3.56E-01	7.79E-02
General Plastics FR-6710 Polyurethane Foam [7]	8.60E-02	8.60E-02	8.60E-02	3.31E-02	3.31E-02	3.31E-02	3.00E-01	3.00E-01	3.00E-01
HRH-10-1/8-8 Nomex Honeycomb [8]	2.58E-03	7.89E-04	5.38E-01	2.00E-04	1.10E-01	6.55E-02	1.8E+00	1.27E-03	2.65E-01

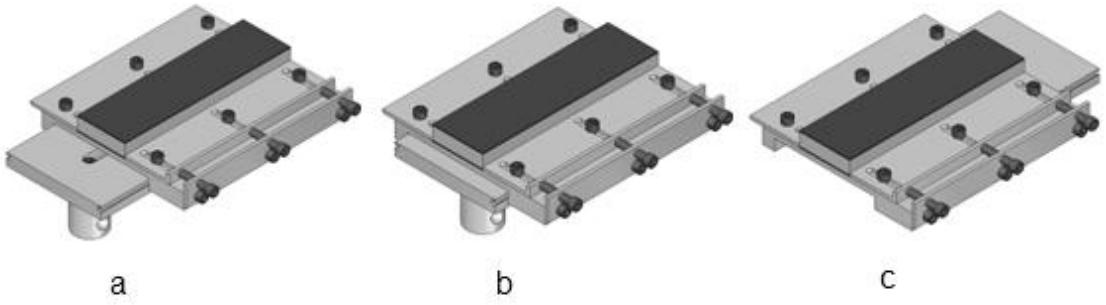

Figure 3-3: Translating fixture showing the base plate's ability to translate

horizontal translation, the specimen could translate forward as the debond propagated, allowing for a more vertical loading path. During coupon testing it was seen that as the debond grew, the base support translated forward as planned. However, a concern developed that this forward shifting of the base support could affect debond growth. The inertia associated with the forward movement of the base support could introduce horizontal, or shear loading components at the debond front. This Mode II loading would be difficult to quantify and would decrease the Mode I dominance, defeating the original purpose of the translating base.

The second method to ensure vertical loading was to offset the load through the use of a lengthened loading rod. As shown in Figure 3-4(b), by increasing the length of the loading rod, *L*, the rod rotation, α, is decreased. This is shown mathematically in Equations 3.1- 3.3. When the loading rod is sufficiently long, even as the debond length, *a*, increases then α is minimized to a sufficient amount that it can be assumed that the load application remains essentially vertical [2].

$$L_{BB'} \approx 2a \sin\frac{\theta}{2}$$

Equation 3.1

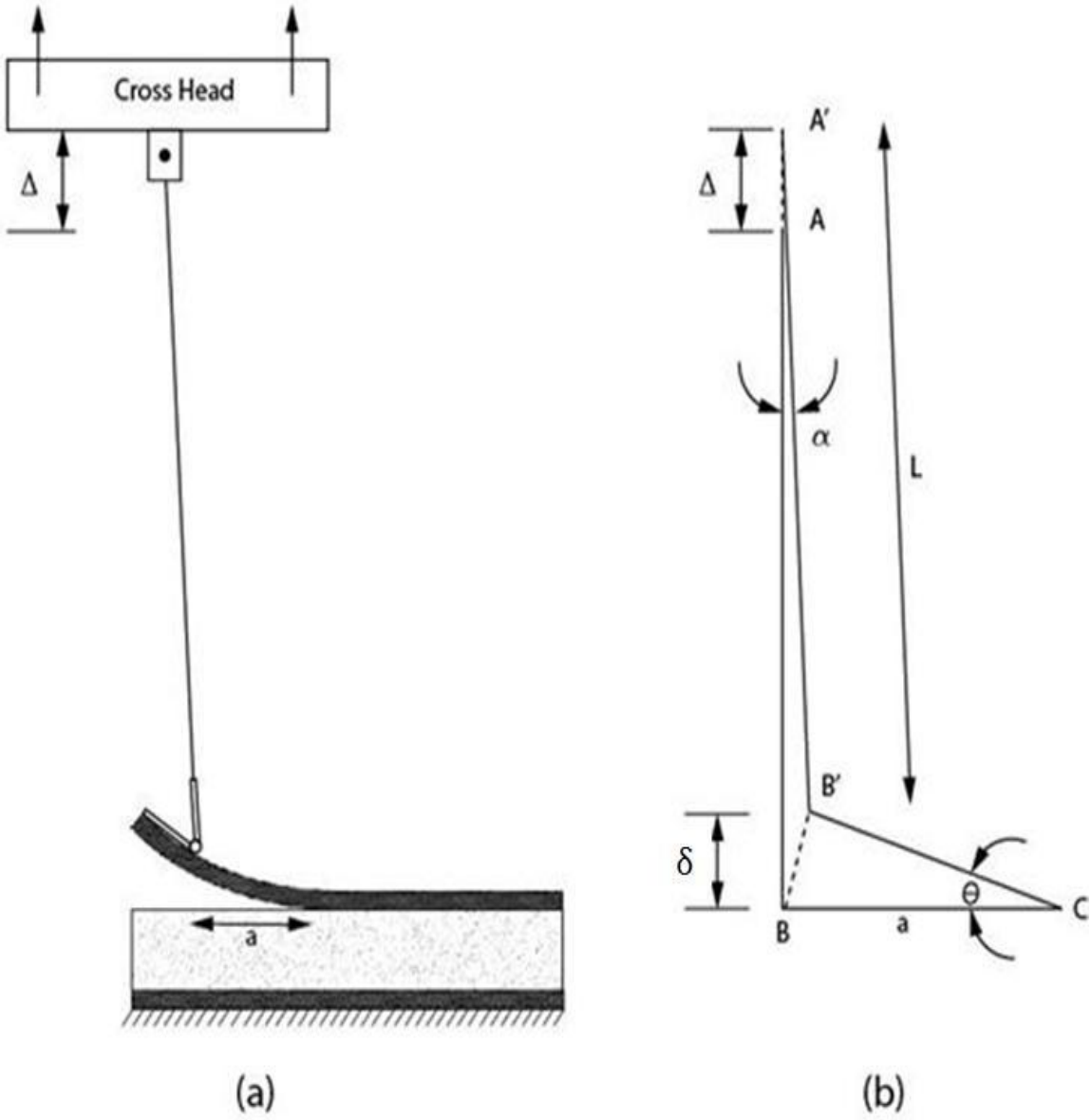

Figure 3-4: (a) Load setup showing offset load application using a loading rod (b) Load application kinematics

$$\theta \approx \sin^{-1}\frac{\delta}{a}$$

Equation 3.2

$$\alpha \approx \cos^{-1}\left[\frac{L^2 + (L+\delta)^2 - L_{BB'}^2}{2L(L+\delta)}\right]$$

Equation 3.3

To further investigate the use of a lengthened loading rod, the same FE model which was used previously while analyzing the translating base fixture was modified by adding a loading rod through which the vertically applied load was applied. Pin connections were used to connect the loading rod to the facesheet so as not to cause moments. The lower facesheet was fully constrained in both the x and y directions to simulate the coupon being fixed to the non-translating base plate. Finite element analysis showed an increased Mode I loading percentage at the debond front when the loading rod was used, just as it did with the translating base plate.

A comparison of the analysis results was made between these three methods of test fixturing; the un-altered specimen, which was fully constrained in the x and y directions and had the load applied directly to the facesheet, the translating base method, and the offset load application (loading rod) method. It was found that both the translating base and loading rod test configurations had increased Mode I dominance over testing performed on the unaltered specimen. These results also showed that when no alterations were made to either the specimen constraint or load application methods then Mode I dominance decreased as debond length increased, as shown in Figure 3-5. Similarly, it was found that by either allowing the base support to translate or by offsetting the load application point through use of a loading rod, a higher and more consistent Mode I loading percentage was present at the debond front. This was the case

for analyses performed at all debond lengths; the translating base and loading rod increased Mode I loading.

Although testing using the translating base and testing using the loading rod yielded similar test results, the loading rod fixturing eliminated the inertial issues without affecting the Mode I dominance at the debond front. Additionally, the use of the loading rod was less complicated. Thus, the use of a lengthened loading rod was selected as the preferred load application method. However, the translating base method is still considered acceptable.

3.2.1 Minimum Rod Length

As was shown in Figure 3-4, increased loading rod length minimizes loading rod rotation which, in turn, minimizes the Mode II component of G_c. To determine the minimum loading rod length which will guarantee high Mode I dominance, Ratcliffe

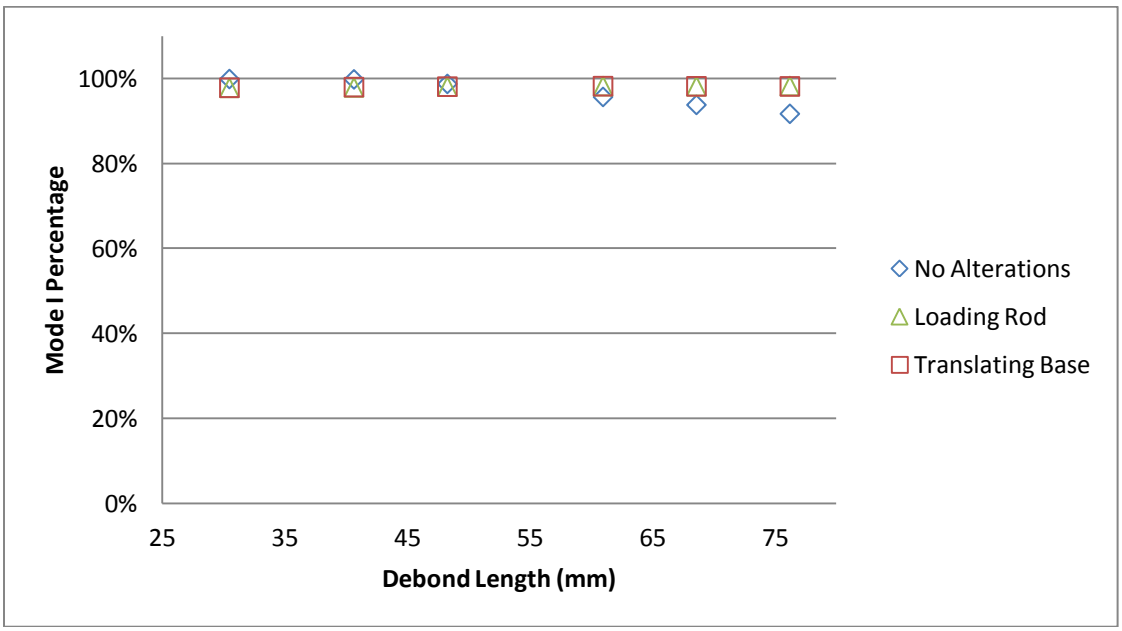

Figure 3-5: Mode I loading percentages at the debond front vs. debond length for different test configurations

explains that there are some assumptions which can be made to simplify the calculations. He explains that it can be assumed that the debonded facing undergoes no axial deformation and the vertical displacement of the specimen load point is equal to the translation of the crosshead [2]. When these assumptions are made, then the minimum loading rod length can be estimated by

$$L_{min} \approx 1.062 a_{max}.$$

Equation 3.4

In this equation he defines a_{max}, the maximum debond length, as the sum of the initial debond length, a, and the amount of debond growth seen during the test, a_{prop}. This is shown mathematically in Equation 3.5:

$$a_{max} = a + a_{prop},$$

Equation 3.5

where a is the larger of the Equations 3.6 and 3.7.

$$a_{min}^{compliance} = 2.7 \left[\frac{t_c t_f^3 E_f}{3E_f} \right]^{\frac{1}{4}} = L_{b,min}$$

Equation 3.6

$$a_{min}^{bending} \approx \sqrt{\frac{30 E_f t_f^2}{G_{xz,f}}} - .59 L_{b,min},$$

Equation 3.7

where t_c is the core thickness, t_f is the facesheet thickness, E_f is the facesheet flexural modulus, $G_{xz,f}$ is the facesheet shear modulus, and $L_{b,min}$ is the minimum specimen length for a SCB specimen. Past research [2] has shown adequate a_{prop} values for specimens which exhibit stable debond growth to be approximately 50.8 mm (2.0 in.) and 76.2 mm (3.0 in.) for specimens which experienced unstable debond growth. This

unstable or stick-slip debond growth is characterized by short sudden occurrences of debond growth rather than steady, consistent growth.

Using Equation 3.4, it was determined that for the testing conducted throughout this research a 203 mm (8.0 in.) loading rod was sufficient to provide a Mode I dominated loading condition at the debond front. Less than 5% difference was seen between the G_c values obtain in testing using the loading rod and testing using the translating carriage.

4 SPECIMEN WIDTH EFFECTS

Test specimen width is an important parameter in testing the interlaminar fracture toughness of a sandwich composite. If the specimen is too narrow, it is possible that curvature of the debond could result in inaccurate G_c measurements. On the other hand, if specimen width is too great, then larger test panels are required, and past a certain point it is likely that there is no benefit in increased specimen width. An optimal specimen width was investigated; a practical width that delivers accurate test results and minimizes material costs.

4.1 Debond Curvature

Debond curvature is one element that affects specimen width. Ideally, the debond front across the width of a specimen would be a straight line, perpendicular to the edges of the specimen which would remain straight as the debond propagated. An un-curved, unchanging debond, such as the one described, would signify that a constant G_c was present at every point of the debond across the width of the specimen. Although this scenario would be preferred, it was found during this research that varying degrees of debond curvature existed for different sandwich configurations. The main contributor to the degree of debond curvature was found to be anticlastic curvature of the facesheet.

Anticlastic curvature is a Poisson's ratio induced deformation that causes a transverse, or saddle shaped, curvature to develop when a bending moment is applied to the facesheet. These anticlastic effects are more pronounced in laminates with high in-

plane Poisson's ratio (ν_{12}) properties and nonzero D_{16} and D_{26} terms, such as $[\pm 45]_S$ laminates. Sandwich composites constructed using facesheets with high ν_{12} properties will therefore see increased degrees of debond curvature over facesheets with low ν_{12} properties, as shown in Figure 4-1.

Although it is known that certain facesheet layups will result in increased debond curvature, there are certain applications where these facesheet layups are preferred. In these situations, little can be done to alter the fiber orientation of the facesheet to reduce the amount of debond curvature that will be present during testing. It may not be preferred to change the fiber orientation of the test coupon in an attempt to reduce debond curvature, as the data obtained would not be representative of the sandwich configuration of interest. In this case it would be necessary to accept the presence of the curved debond and proceed with testing.

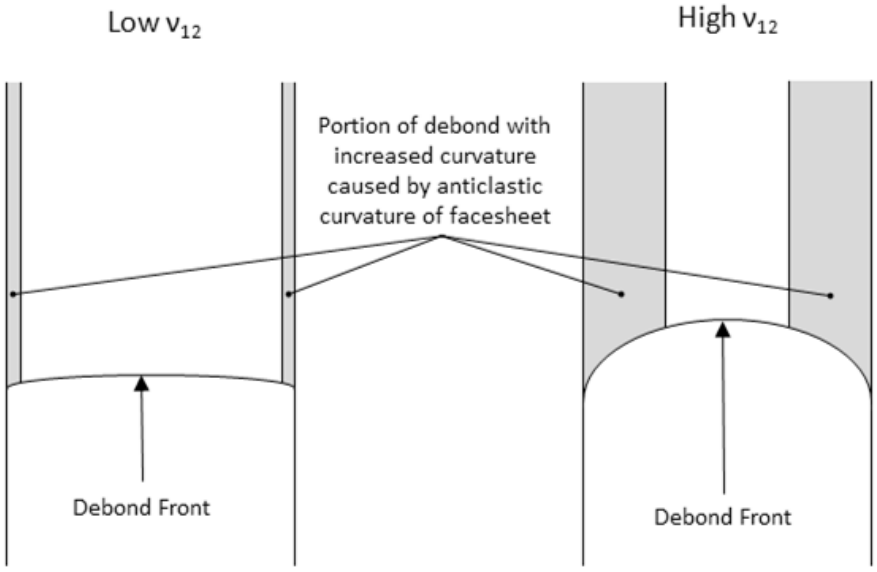

Figure 4-1: Thumbnail shaped debond front showing regions of curvature caused by free edges and anticlastic curvature of the facesheet

This issue is not unique to sandwich composites; it is present with laminates as well. Prior to the standardization of ASTM D 5528, a study was preformed which investigated the strain energy release rate of a DCB laminate coupon [12]. Results of this study suggested that accurate G_c results could be achieved, despite the debond curvature which existed during testing, so long as certain conditions were met. The first of these conditions was ensuring self similar debond growth had been met. Self-similar debond growth is defined as growth in which the shape and degree of curvature of the debond front remains unchanged as the debond propagates. The second condition was fully developed debond growth. Fully developed debond growth is achieved once the length of the debond is sufficient that G_c measurements at a given distance from the edge do not change as the debond propagates. For example, consider the case where G_c measurements are made at a distance *d* from the edge of the specimen when the debond length was *a* and again when the length was increased to $a+\Delta a$. For fully developed debond growth, these two measurements of G_c made at the same distance *d* from the edge would be the same.

Therefore, by allowing the debond to reach a state of fully developed, self similar debond growth, accurate G_c measurements can be obtained, despite the presence of the curvature in the debond.

4.1.1 Finite Element Analysis of Specimen Width

To investigate the variation of debond curvature, a three-dimensional finite element model was constructed and analyzed in ANSYS using eight-noded isoparametric SOLID45 elements with 3 degrees of freedom at each node. The specimen model was 178 mm (7.0 in.) long with a core thickness of 12.7 mm (0.50 in.) and a facesheet

thickness of 1.27 mm (0.05 in.). There were 140 elements along the length of the model, 10 elements through the thickness of the core, and a single element through the thickness of each facesheet. Specimen width for this study was 25.4 mm (1.0 in.), however computation was reduced through the use of the plane of symmetry existing along the mid-plane of the specimen (z = 0), and only one-half of the specimen was modeled. Across this width, there were 10 elements modeled, creating a total of 16,800 elements as shown in Figure 4-2. The material properties listed in Table 3-1 were used for this three-dimensional analysis.

As was done with the two-dimensional FEA, the facesheets were connected to the core by merging the nodes along the interfaces. The debond was modeled by coupling the nodes of the facesheet and core at the desired location. The lower facesheet was fully constrained, preventing translation and rotation, and simulating the specimen being clamped in the base of the test fixture. The solution was obtained with geometric nonlinearity enabled.

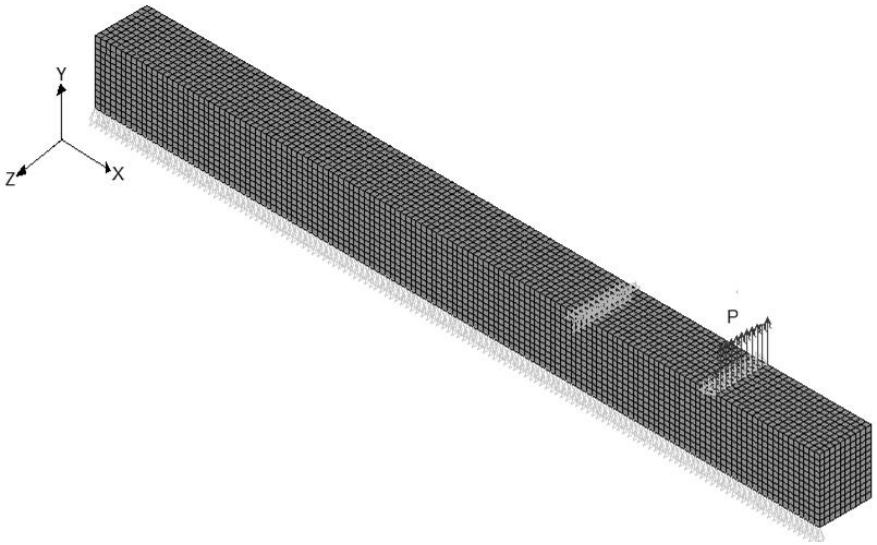

Figure 4-2: Orientation and mesh of finite element model

Through the use of three-dimensional analysis it was possible to capture the degree of curvature of the debond front. By inputting the material properties of different facesheet layups into the finite element code it was possible to evaluate the effects that facesheet ply orientation have on debond growth. Based on the results of these analyses, coupon testing was performed and the proper test specimen width could be selected.

Facesheet ply orientation effects were evaluated by modeling a straight debond in the finite element model and evaluating the normal stresses in the out-of-plane Y-direction across the width of the debond. By evaluating these stresses at each node across the specimen width, the degree of curvature could be captured for sandwich composites with both quasi-isotropic and cross-ply facesheets.

Analysis was performed for each specimen, and the normal stresses across the width of the debond were plotted as functions of distance from the specimen edge, as seen in Figure 4-3. These results revealed that variation in normal stress across the debond front was greater for quasi-isotropic facesheeted sandwiches than it was for cross-ply sandwich specimen. This increased variation in stress indicates that sandwich composites with quasi-isotropic facesheets will exhibit greater debond curvature than those with cross-ply facesheets.

This increase in debond curvature for sandwich composites with quasi-isotropic facesheets is due to the increased anticlastic bending undergone by the facesheets as they are deflected upward. Laminated plate theory shows quasi-isotropic laminates to have much higher ν_{12} ratios than cross-ply laminates; 0.23 compared to 0.04, respectively. As a result of these higher Poisson's ratios, the quasi-isotropic facesheets experience greater

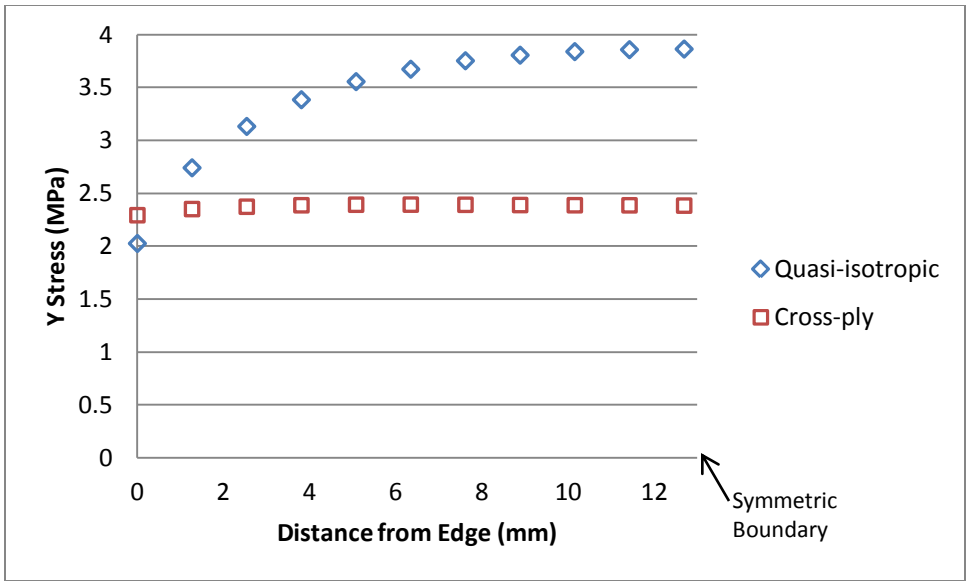

Figure 4-3: Normal stress in the core of a foam sandwich specimen with quasi-isotropic and cross-ply facesheets.

anticlastic deformation under bending and, subsequently, increased curvature of the debond front.

In addition to ply orientation, the combined effects that facesheet and core stiffness have on the shape of the debond front were investigated. Independently of each other, facesheet and core stiffness properties were varied and G_c was evaluated. At each node across the width of the debond, a ratio of G_{c_i} (at the node of interest) to $G_{c_{middle}}$ (at the center of the specimen) was found. By plotting this ratio, $G_{c_i}/G_{c_{middle}}$, for each node as a function of distance from the specimen edge, the degrees to which the facesheet and core stiffness affected G_c and, consequently, debond curvature were determined. By so doing, it was determined how each of the sandwich construction constituents contributed to the shape of the debond front.

Using the foam core sandwich configuration described in Table 2-1 as a control, the core stiffness was increased by multiplying the modulus by factors of 2.5 and 5. The

by factors of $^{2}/_{5}$ and $^{1}/_{5}$. Individually, these altered core modulus properties were input into the model and the results were compared with each other. It was found that as core stiffness was increased, variation in $G_{c_i}/G_{c_{middle}}$ increased as well, represented by the series "Core X 2.5" and "Core X 5" shown in Figure 4-4. As the core stiffness was decreased, represented by the series "Core X 2/5" and "Core X 1/5", the variation of $G_{c_i}/G_{c_{middle}}$ decreased across the width of the specimen. This correlates to an increase in debond curvature when the core stiffness is increased and a decrease in debond curvature when core stiffness is decreased.

Following the same method, the facesheet stiffness was varied while the core properties were held constant. The facesheet stiffness was increased by multiplying the facesheet axial modulus by factors of 2.5 and 5, represented by series "FS X 2.5" and "FS

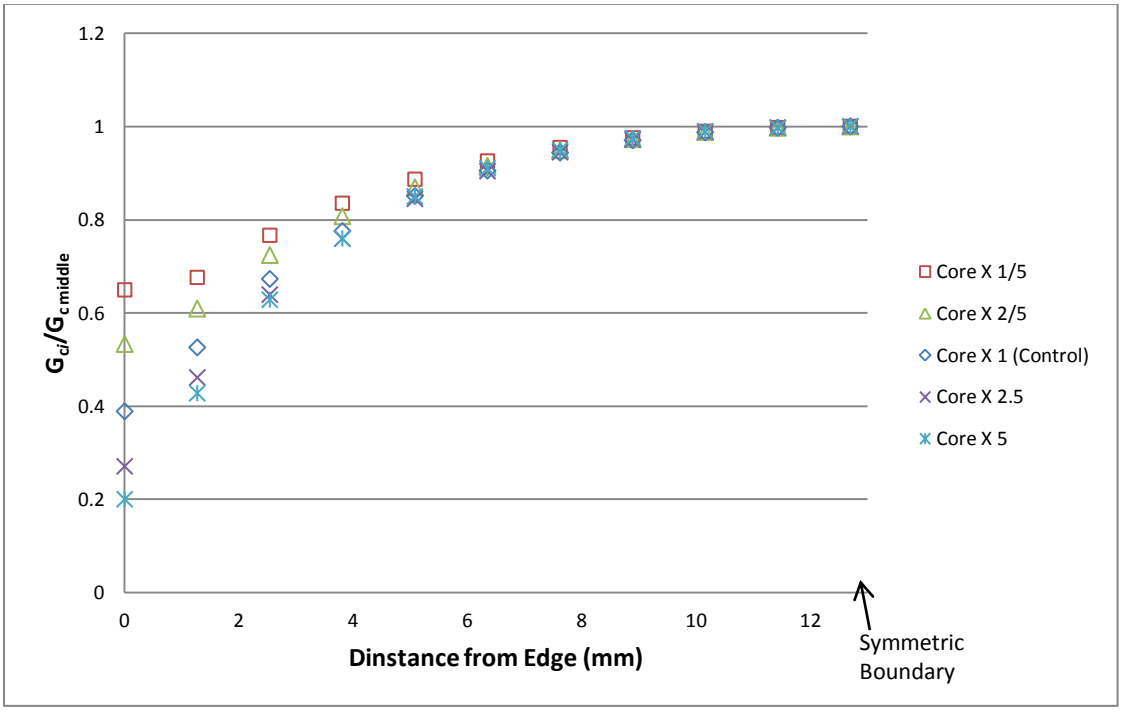

Figure 4-4: Variation in $G_{ci}/G_{c\,middle}$ at debond front across the width of specimen with different core moduli

X 5" shown in Figure 4-5. The facesheet stiffness was decreased by multiplying the axial modulus of the facesheets by factors of $^2/_5$ and $^1/_5$, represented by "FS X 2/5" and "FS X 1/5". The results, displayed in Figure 4-5, show that increasing the facesheet stiffness causes a decrease in variation of G_c across the width of the specimen. By decreasing facesheet stiffness, variation in G_c across the width of the specimen was increased. This signifies that debond curvature is amplified when the facesheet stiffness is decreased and that debond curvature is reduced when facesheet stiffness is increased.

Based on these findings, shown in Figure 4-4 and Figure 4-5, it can be seen that increasing core and facesheet stiffnesses affect debond curvature differently: stiffer cores will increase debond curvature while stiffer facesheets will decrease it. It can also be seen that the degree to which $G_{c_i}/G_{c_{middle}}$ fluctuates is greater when facesheet stiffness is

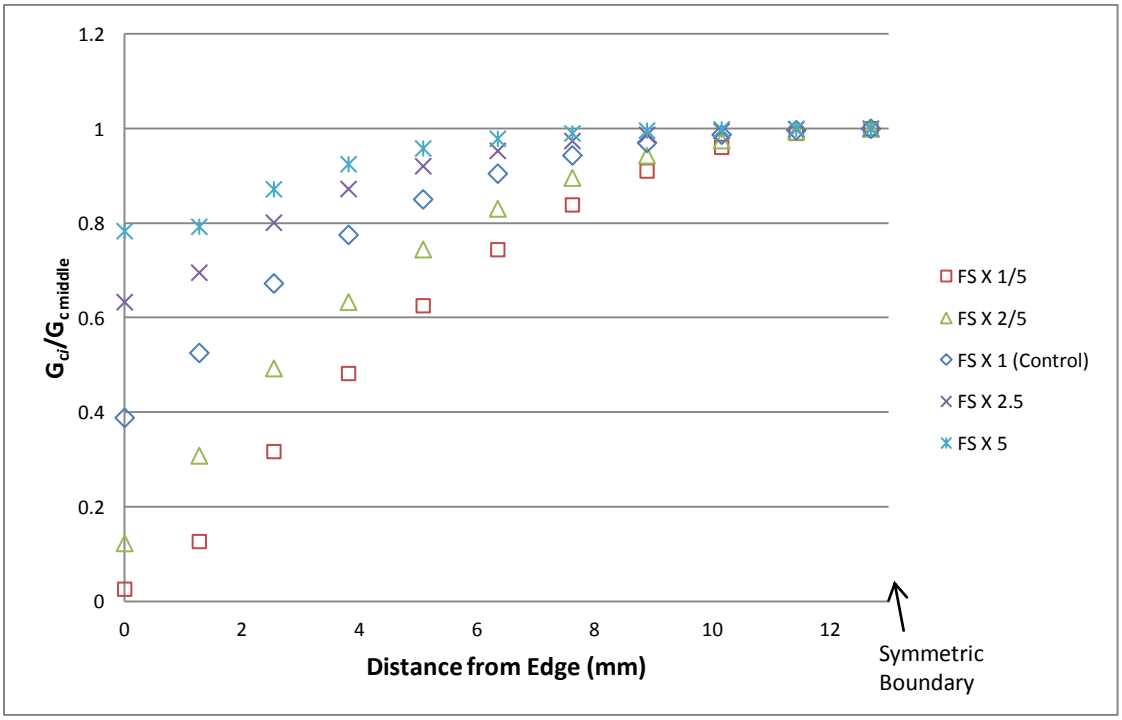

Figure 4-5: Variation in $G_{ci}/G_{c\,middle}$ at debond front across the width of specimen with different facesheet axial moduli

varied than when the core stiffness is varied. This result is due to the anticlastic curvature of the facesheet, and how this saddle-shaped curvature contributes to debond shape. When facesheet stiffness is decreased, the facesheet undergoes increased deflection and bending prior to debond growth. This increased bending correlates to increased anticlastic curvature of the facesheet, leading to increased debond curvature. Therefore, by altering the compliance of the facesheet, the amount of anticlastic curvature the facesheet undergoes is also altered.

In summary, debond curvature is affected by both facesheet stiffness and facesheet laminate layup. The results obtained from this analysis imply that a relatively compliant, quasi-isotropic facesheet would see greater amounts of debond curvature than a relatively stiff, cross-ply facesheet. This result suggests that without changing the layup of a facesheet, the amount of debond curvature could be reduced by increasing its flexural stiffness. Such stiffness increase could be accomplished through the bonding of a doubler to the facesheet. This concept, applying bonded doublers to compliant facesheets to improve G_c measurements is discussed in greater detail in Section 5.

4.1.2 Specimen Width Test Results

Three widths of foam sandwich panels and two facesheet configurations were selected to evaluate specimen width effects. These widths were 25.4 mm (1.0 in.), 50.8 mm (2.0 in.) and 76.2 mm (3.0 in.). The two facesheet configurations were $[(0/90)/(\pm 45)]_{3T}$ quasi-isotropic facesheets and $[(0/90)_2]_S$ cross ply facesheets, as specified in Table 2-1. Following the Mode I interface fracture toughness test standard contained in Appendix B and using the test SCB fixture developed by the University of Utah

described in Section 3, three specimens of each width and each facesheet configuration were tested. The results of this testing are shown in Figure 4-6 and Figure 4-7.

Focusing specifically on the quasi-isotropic facesheet results shown in Figure 4-6, it can be seen that G_c measurements for the narrowest specimens tested, the 25.4 mm (1.0 in.) wide coupons, did not stabilize. Rather, G_c measurements continued to increase as the debond propagated. The 50.8 mm (2.0 in.) and 76.2 mm (3.0 in.) specimen, on the other hand, saw more consistent G_c measurements throughout the test; approximately 0.19 N/mm. It is believed that the increasing G_c results of the 25.4 mm (1.0 in.) specimen are due to the anticlastic deformation which the quasi-isotropic facesheets underwent as the coupons were tested. At this narrower width, the majority of the debond front was being affected by the curvature of the debond along the edges of the specimen. When the specimen width was increased to 50.8 mm (2.0 in.) and 76.2 mm (3.0 in.) however, it can be seen that a more constant value of G_c was measured at all debond lengths. Although the quasi-isotropic facesheets of these wider specimen still underwent anticlastic deformation, the added width allowed for a more fully developed debond front and a larger percentage of the debond front was unaffected by the curvature at the edges. For this reason the G_c measurements were more consistent for the wider specimen.

Results from the specimens with cross-ply facesheets, shown in Figure 4-7, show consistent G_c measurements for all three coupon widths. Since the cross-ply facesheets are less susceptible to anticlastic deformation, there was less debond curvature and more consistent data was gathered for specimens of all widths.

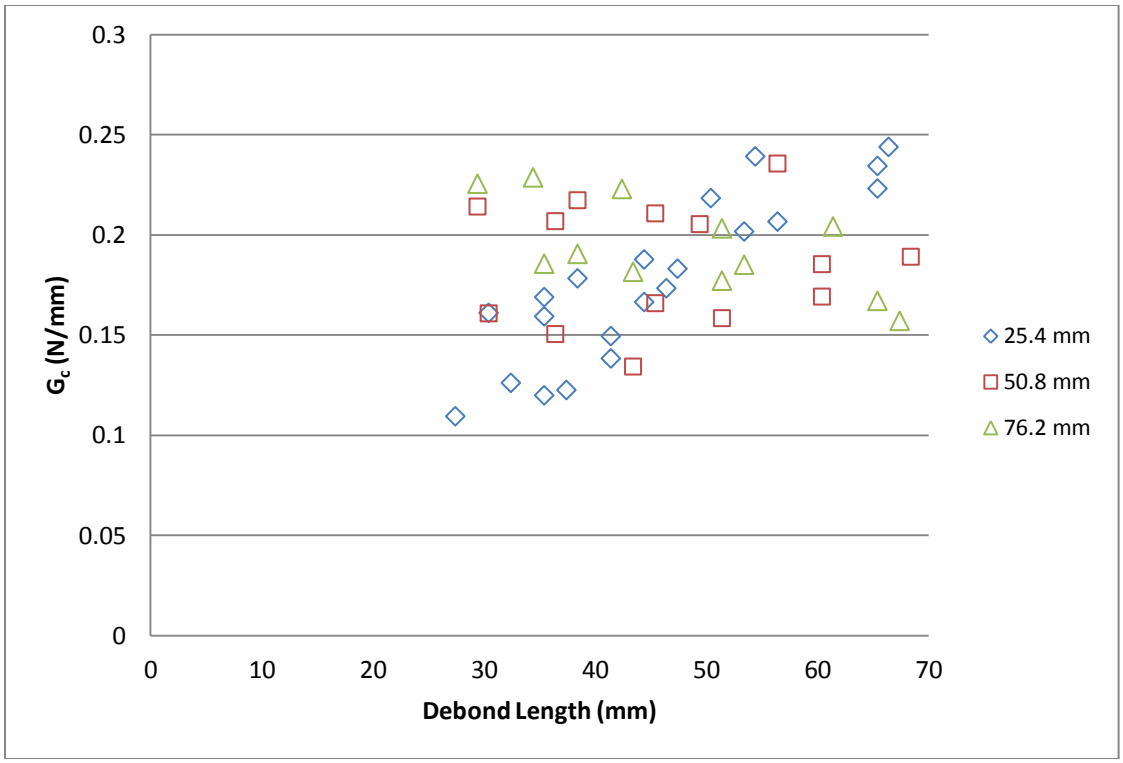

Figure 4-6: G_c vs. debond length for foam specimen with quasi-isotropic facesheets

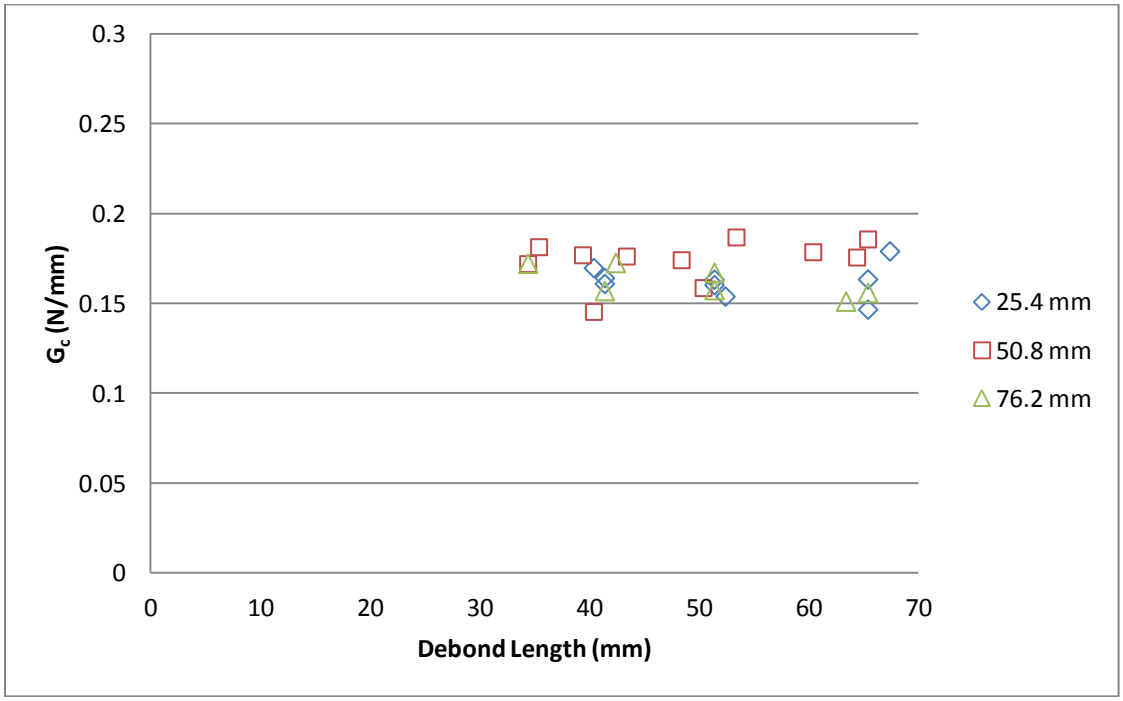

Figure 4-7: G_c vs. debond length for foam specimen with cross-ply facesheets

To further evaluate the shape of the debond front, a dye penetrant developed by the University of Utah Composite Mechanics Laboratory was used to visually assess the debond curvature for specimens of different widths and facesheet configurations [13]. This penetrant is made by combining equal parts of isopropyl alcohol and liquid film developer with a few drops of black fountain pen ink. During testing, the liquid penetrant was introduced to the debond and allowed to wick to the debond front. The coupons were then removed from the test fixture and the penetrant was allowed to dry. The facesheets were then peeled from the core, and the dye clearly indicated the shape of the debond and the amount of curvature present for each of the sandwich configurations. The results from the dye penetrant experiments are shown in Table 4-1 and indicate that debond curvature is more prevalent with quasi-isotropic facesheets than for cross-ply facesheets. These findings are in agreement with the FEA results discussed previously which showed greater debond curvature along the edges of the quasi-isotropic specimen than the cross-ply specimen.

In summary, results from finite element analysis and mechanical testing suggest that both specimen width and facesheet lay-up can affect G_c measurements. Based upon these findings, it is suggested that a minimum specimen width of 50.8 mm (2.0 in.) be specified for all SCB testing. Although anticlastic deformation of the facesheet increases the degree of curvature of the debond front, a 50.8 mm (2.0 in.) specimen width appears to be sufficient for both cross-ply and quasi-isotropic facesheet layups.

4.2 Honeycomb Cell Size

Thus far, focus has been placed upon foam cores, which have a continuous bond surface. However, discontinuous bond surface cores, such as honeycomb, are commonly

Table 4-1: Debond front curvature for quasi-isotropic and cross-ply foam sandwich specimen of varying widths

Width (mm)	Quasi-isotropic	Cross-ply
25.4	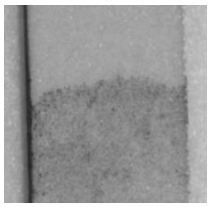	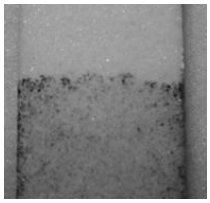
50.8	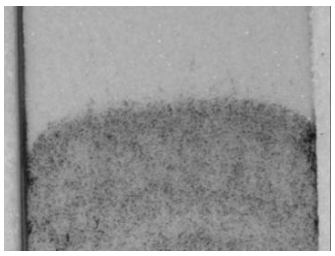	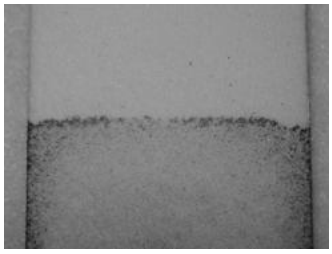
76.2	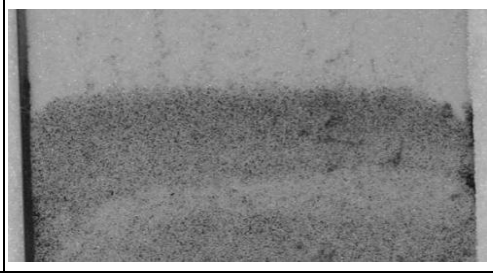	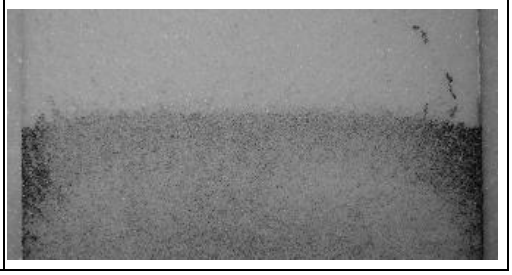

used in sandwich constructions as well. Due to the fact that the bond surface of a honeycomb core is not continuous, a more complex debonding condition can exists where G_c, at a given location across the debond front, can vary depending on the number of cells through which the debond is required to propagate. Concerning test standard development, even when a minimum specimen width is specified, if there are too few cells across the width of a honeycomb test coupon, inaccurate G_c measurements may result. For example, if the bond contact area between the core and facesheet across the crack front is low, as seen in Figure 4-8 (a), then G_c measurements will be reduced. Similarly when the crack front is located at a position of the honeycomb with higher

bonding area, as shown in Figure 4-8 (b), G_c measurements could be higher. It is therefore necessary to specify not only a minimum specimen width, but also a sufficient number of cells across the width of a honeycomb-cored specimen.

Previous studies have suggested that six cells across the width of a honeycomb sandwich coupon are sufficient to achieve consistent G_c measurements [2 and 3]. Due to the computational complexity required to model a honeycomb bonding surface, no finite element analyses were performed to investigate this topic. However, a series of tests were performed to determine the minimum number of honeycomb cells required across the specimen width.

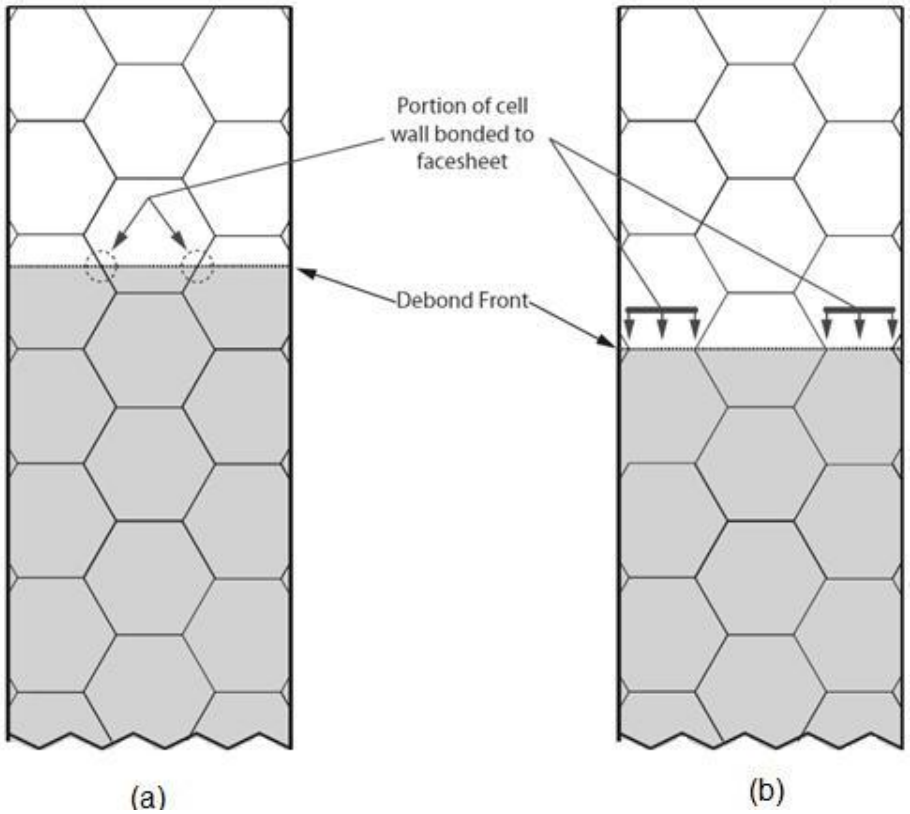

Figure 4-8: Honeycomb specimen with (a) low percentage of cell wall bonded to facesheet and (b) high percentage of cell wall bonded to facesheet

4.2.1 Cell Size Coupon Testing

Two honeycomb core sandwich configurations were tested, aluminum and Nomex, as listed in Table 2-2. Testing was performed using a 9.53 mm (0.38 in.) cell sized honeycomb core. By using a rather course cell size, it was hoped that width effects caused by cell size would be more pronounced and more easily captured during testing. The Nomex and aluminum cored sandwiches were cut into specimens with widths of 25.4 mm (1.0 in.), 50.8 mm (2.0 in.) and 76.2 mm (3.0 in.). This correlated to coupons with approximately 3, 6, and 8 full cells across the width of each coupon.

As was done with the foam core sandwich coupons, testing for the honeycomb core sandwich coupons was carried out on the previously described SCB test fixture following the SCB test standard draft which is contained in Appendix B. The results for the aluminum core and Nomex core testing are shown in Figure 4-9 and Figure 4-10 respectively.

Through inspection of Figure 4-9, it appears that the narrow 25.4 mm (1.0 in.) specimen width produced increased scatter versus the 50.8 mm (2.0 in.) and 76.2 mm (3.0 in.) wide specimen. Average G_c values and standard deviations were calculated for the three specimen widths and are displayed in

. As specimen width was increased from 25.4 mm (1.0 in.) to 50.8 mm (2.0 in.), both the average G_c and standard deviation decreased slightly. Increasing the coupon width from 50.8 mm (2.0 in.) to 76.2 mm (3.0 in.) brought another decrease in standard deviation, however no significant change was observed in the average G_c. These results suggest that fewer cells across the specimen width will result in increased scatter, and that as the number of cells across the width is increased, the degree of scatter is reduced. Further,

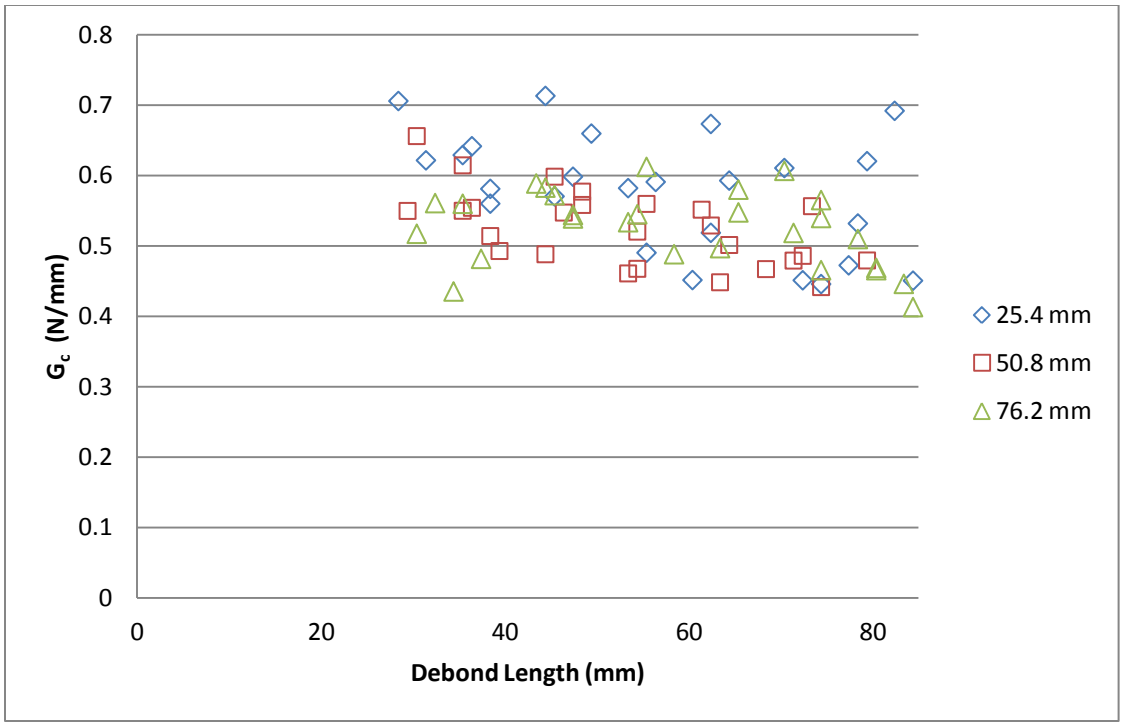

Figure 4-9: Aluminum honeycomb width test results

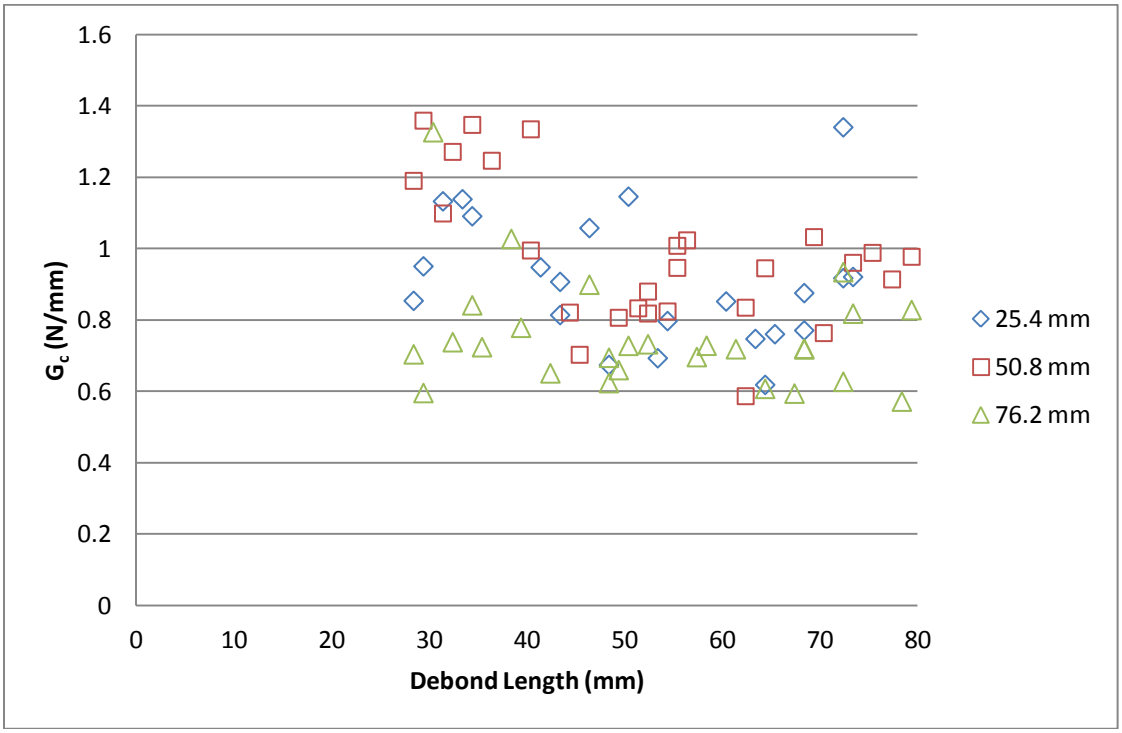

Figure 4-10: Nomex honeycomb width results

these results suggest that a 50.8 mm (2.0 in.) wide specimen with six complete unit cells will deliver similar results to a 76.2 mm (3.0 in.) wide specimen with eight complete unit cells, suggesting that the added width beyond six unit cells may not be necessary for testing honeycomb core sandwich composites.

The Nomex honeycomb test results showed much more scatter than the aluminum honeycomb, as can be seen by comparing Figure 4-9 and Figure 4-10. Averages and standard deviations were calculated for the Nomex core as for the aluminum core specimen and these results are displayed in Table 4-3. As specimen width was increased the scatter was reduced, as shown by the decrease in standard deviation. However, average G_c values were changed significantly as specimen width increased. Upon examination of the debond paths in the Nomex specimens, it was noticed that rather than the debond propagating along the upper surface of the core, as was the case with the aluminum specimen, there were areas along the debond where small fragments of Nomex

Table 4-2: Average G_c and standard deviation for aluminum honeycomb sandwich composite specimens of different widths

Specimen Width (mm)	G_c Average (N/mm)	G_c Standard Deviation (N/mm)
25.4	0.58	0.09
50.8	0.52	0.06
76.2	0.52	0.05

Table 4-3: Average G_c and standard deviation for Nomex core sandwich composite specimens of different widths

Specimen Width (mm)	G_c Average (N/mm)	G_c Standard Deviation (N/mm)
25.4	0.91	0.22
50.8	0.93	0.18
76.2	0.78	0.16

were still bonded to the debonded facesheet. This signifies that at times the debond grew through portions of the cell walls of the Nomex honeycomb. Further examination revealed many of the spikes in the G_c data seen in the early portions of debond growth appear to correlate to the areas where Nomex fragments were seen still attached to the debonded facesheet. Examination of previous testing involving Nomex honeycomb cores showed increased amounts of scatter when compared to identical testing performed on foam core and aluminum honeycomb core sandwich composites [6].

The results obtained from testing honeycomb core sandwich specimens with different widths support the aforementioned claim that a minimum of 6 honeycomb cells across the width of a coupon are desired. However, in addition to the minimum cell requirement, it is also recommended that a minimum width of 50.8 mm (2.0 in.) be placed upon SCB test specimens. By placing this minimum width requirement, potential problems associated with high Poisson's ratio facesheets may be minimized. This minimum width may be increased as necessary to ensure that the additional minimum cell requirement is satisfied.

5 THIN FACESHEET EFFECTS

A key advantage of using sandwich composites is the structural stiffness that can be achieved, even when very thin facesheets are used. These thin facesheets, although quite compliant, are capable of creating a very stiff, light weight structure when bonded to a core. Paradoxically, while thin facesheets assist in forming a lighter weight structure with a high specific stiffness, they create difficulty when performing the SCB test and reducing the test data using the Compliance Calibration (CC) method due to the large rotations which the facesheets undergo during testing.

The CC method is one of the more commonly used data reduction techniques to measure G_c [6]. In performing a SCB test, the facesheet onto which the load is being applied can be thought of as a cantilever beam whose length is equal to that of the debond. As the debond grows, the cantilevered length of the beam increases which, in turn, changes the compliance of the beam. The CC solution relies upon this change in facesheet compliance to calculate G:

$$G = \frac{dU}{da} = \frac{P^2}{2W}\frac{dC}{da},$$

Equation 5.1

where P is the applied load, W is the specimen width, a is the debond length, and C is the compliance of the facesheet found using the expression:

$$C = \frac{\delta}{P},$$

Equation 5.2

where δ is the load point displacement. By plotting C as a function of debond length, a CC coefficient can be found following the popular Berry method [14, 15, 16, and 17]:

$$C = ba^m$$

Equation 5.3

Inserting Equation 5.3 into Equation 5.1 results in:

$$G = \frac{P^2}{2W} mba^{m-1}$$

Equation 5.4

where m and b are the CC curve-fit coefficients.

Ratcliffe, however, explains that the compliance solution is based upon beam theory, which relies upon small displacement assumptions [2]. He theorizes that if the facesheet is too thin or compliant, then displacements will be excessive, and specimen response will violate the small displacement assumptions. When these small displacement assumptions are violated, inaccurate G_c measurements will result. Thus, based on previous analysis of DCB laminate specimens, a reasonable deflection limit for the SCB specimen has been set as 20% the length of the debond. Note that this value for the Single Cantilever Beam specimen is half that of the 40% limit specified in the Double Cantilever Beam specimen (ASTM D5528) [2 and 18].

A primary objective of this research was to develop a standardized test method to measure G_c associated with facesheet/core disbond growth in sandwich composites that is suitable for a wide range of sandwich configurations. Given that thin facesheets are not uncommon, the effects of facesheet thickness were examined to determine whether thin facesheet sandwich configurations could be tested using the SCB test method. In this investigation, the focus was to determine whether deflection limits are required, and

whether bonded doublers could be bonded to thin facesheets to reduce deflections and satisfy the 20% deflection restriction. Both finite element analysis and mechanical testing were employed to examine how G_c measurements were affected by facesheet thickness and by the addition of doublers to overly compliant sandwich constructions.

5.1 Analysis of Thin Facesheet Effects

One of the most commonly used techniques for evaluating G numerically is the Virtual Crack Closure Technique (VCCT). This technique is based on Griffith's expression for the energy release rate associated with crack growth [19], given by

$$G = \frac{dW}{da} - \frac{dU}{da},$$

Equation 5.5

where W is the energy required for debond propagation, U is the elastic energy, a is the debond area, and G is the elastic energy release rate. Rybicki and Kanninen [20] modified this expression for use with the finite element method. Following the notation depicted in Figure 5-1, G_I and G_{II} can be calculated using the expressions

$$G_I = \frac{1}{2\Delta a} F_y (v_a - v_b)$$

Equation 5.6

$$G_{II} = \frac{1}{2\Delta a} F_x (u_a - u_b),$$

Equation 5.7

where Δa is the distance between nodes, F_y and F_x are the vertical and horizontal components of the load required to close the crack respectively, v_a and v_b are the

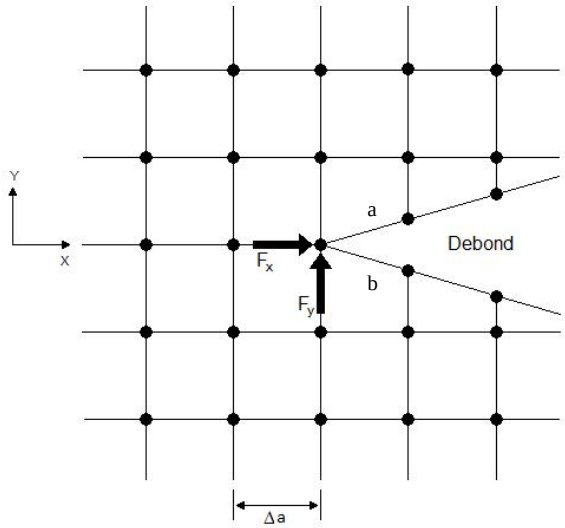

Figure 5-1: Representative finite element mesh used in VCCT

vertical components of the displacements at nodes a and b, and u_a and u_b are the horizontal components of the displacement at nodes a and b.

A series of numerical simulations were performed to evaluate facesheet thickness effects and the use of facesheet doublers to limit deflections in compliant, thin facesheet sandwich configurations, as illustrated in Figure 5-2. The first step involved the development of a compliance vs. debond length curve from which the Compliance Calibration method may be used. A series of initial debond lengths and load point displacements were specified as inputs. From each solution, the load *P* at the application point was obtained. Based on the applied displacement, resulting load, and assumed debond length, a compliance vs. debond length curve was generated. From this curve, compliance calibration coefficients were found using the Berry method.

The second step in the numerical simulation was to simulate the progression of debond growth during testing. For such simulations, an *assumed* value of G_c corresponding to debond growth was required. Next an initial debond length was selected. For the selected debond length and G_c value, the compliance calibration

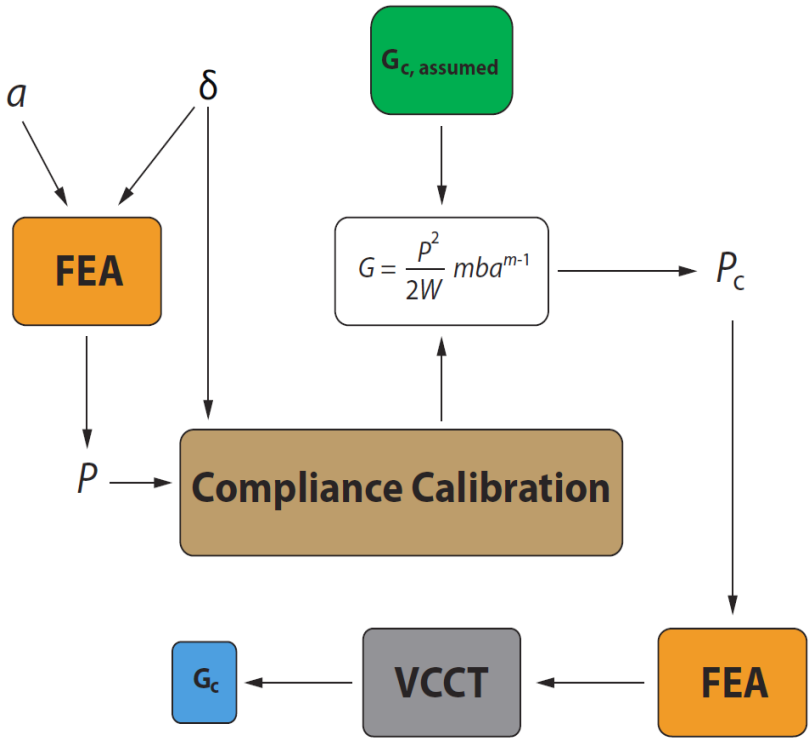

Figure 5-2: Flow chart showing analytical evaluation of Gc using a combination of VCCT and CC methods

coefficients obtained in the first step were used in Equation 5.4 to solve for the critical load, P_c, corresponding to debond growth. This P_c value was used as the input load in a geometrically nonlinear finite element analysis. The resulting G_c value obtained using VCCT was compared to the initial assumed value of G_c to investigate the accuracy of the compliance calibration method, especially for sandwich configurations with thin facesheets and subsequent use of facesheet doublers.

These numerical simulations were performed for three different sandwich configurations; sandwiches that were composed of 0.58 mm (0.02 in.) thick carbon fiber facesheets bonded to 12.7 mm (0.5 in.) thick Nomex honeycomb core, and two of the same sandwich configurations with bonded G-10 glass/epoxy doublers. The two doubler thicknesses used were 0.5 mm (0.02 in.) and 1.6 mm (0.063 in.) thick, as listed in

Table 5-1. For each sandwich configuration, simulations were performed using three different assumed values for G_c; a low value of 0.3 N/mm (1.71 lbf/in.), a medium value of 0.55 N/mm (3.14 lbf/in.), and high G_c value of 0.65 N/mm (3.71 lbf/in.). A 6 ply facesheet construction (which complied with the 20% deflection stipulation previously mentioned) was used as a baseline for comparison.

Results from the numerical simulations are shown in Figure 5-3. As expected, numerical simulation results for the sandwich configuration with the 6-ply facesheets produced G_c values that were in good agreement with the assumed G_c values. In contrast, the sandwich composites with the thinner 3-ply facesheets produced G_c values that were lower than the three assumed values by 11.6%, 20.2%, and 22.7%. Addition of the glass/epoxy doublers to the upper facesheet increased the G_c values from the numerical simulations, reducing the difference with the assumed G_c values as shown. These findings suggest that sandwich configurations with thin facesheets can be modified to produce more accurate Gc values by bonding a doubler to the upper facesheet, thus reducing the facesheet deflection during SCB testing.

5.2 Experimental Evaluation of Thin Facesheet Effects

Following the numerical evaluation of facesheet thickness effects, an experimental evaluation was performed to evaluate the use of facesheet doublers on

Table 5-1: Sandwich configurations for numerical simulations

Config.	Facesheet		Core		Doubler	
	Material	Thickness (mm) [in]	Material	Thickness (mm) [in]	Material	Thickness (mm) [in]
1	Carbon/Epoxy	(0.58) [0.023]	Nomex	(12.7) [0.5]	n/a	n/a
2	Carbon/Epoxy	(0.58) [0.023]	Nomex	(12.7) [0.5]	G-10	(0.5) [0.02]
3	Carbon/Epoxy	(0.58) [0.023]	Nomex	(12.7) [0.5]	G-10	(1.6) [0.063]

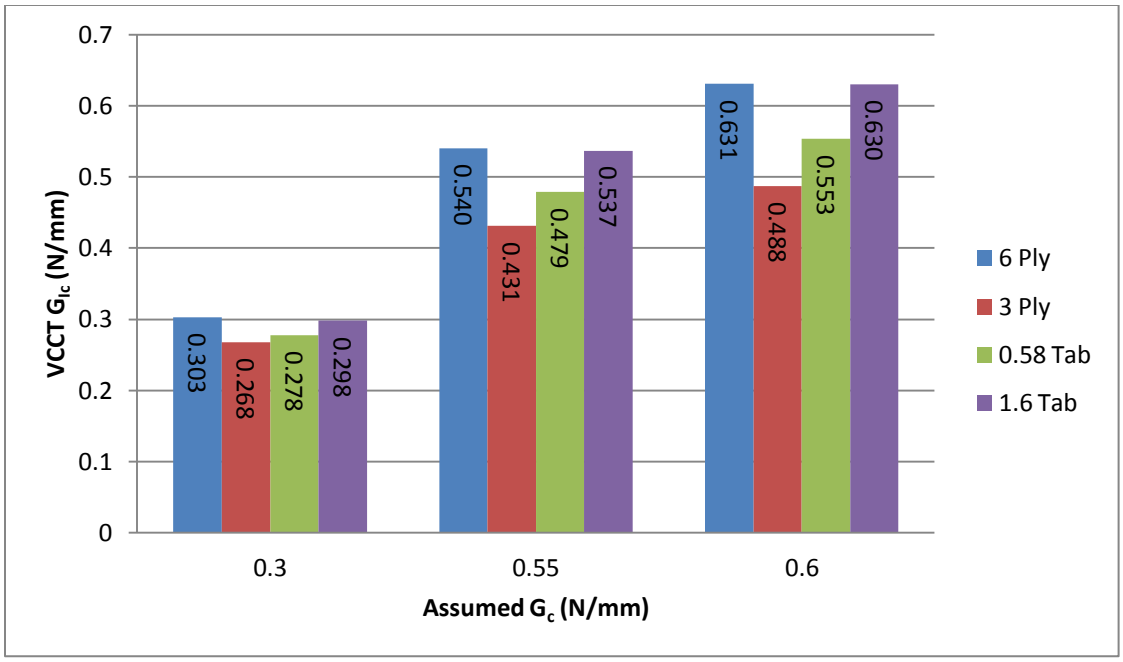

Figure 5-3: Effects of adding tabbing to thin facesheets

sandwich configurations with thin facesheets. For this evaluation, a single sandwich panel of dimensions 229 mm (9.0 in.) x 813 mm (32 in.) was fabricated from 3 ply $[0/90/0]_T$ carbon/epoxy facesheets and Nomex honeycomb core, as outlined in Table 2-2. Following the procedure contained in Appendix A, a 50.8 mm (2.0 in.) wide initial debond was fabricated along the length of the sandwich panel using 0.127 mm (0.0005 in.) thick Teflon film placed between the film adhesive and the core. This panel was then divided into three smaller subpanels of equal size. By using 3 sub-panels, which came from a single "parent" panel, variability in bond strength produced from panel-to-panel variations was reduced. A 0.51 mm (0.02 in.) thick tab was bonded to one of these sub-panels, a 1.6 mm (0.063 in.) thick tab was bonded to the second subpanel and the last subpanel was left without a doubler. Each panel was then cut into five specimen 50.8 mm (2.0 in.) wide. Loading hinges were bonded to the facesheets 25.4 mm (1.0 in.) from the

debond front. The specimens were tested using the SCB Test Method contained in Appendix B.

During testing it was found that each of the groups of tests exhibited failure along the targeted facesheet/core interface without diverting or kinking deeply into the core. However, the failure locations of the three groups varied. The untabbed specimen experienced debonding between the adhesive layer and the facesheet, as seen in Figure 5-4. The 1.6 mm (0.063 in.) tabbed specimen experienced failure in the Nomex honeycomb core at the base of each of the fillets created by the adhesive used to bond the facesheet to the core, as shown in Figure 5-5. The 0.51 mm (0.02 in.) tabbed specimen experienced a combination of the two failure modes with failure occurring at times in the core, along the base of the adhesive fillets, and at other times at the facesheet/adhesive interface, as shown in Figure 5-6.

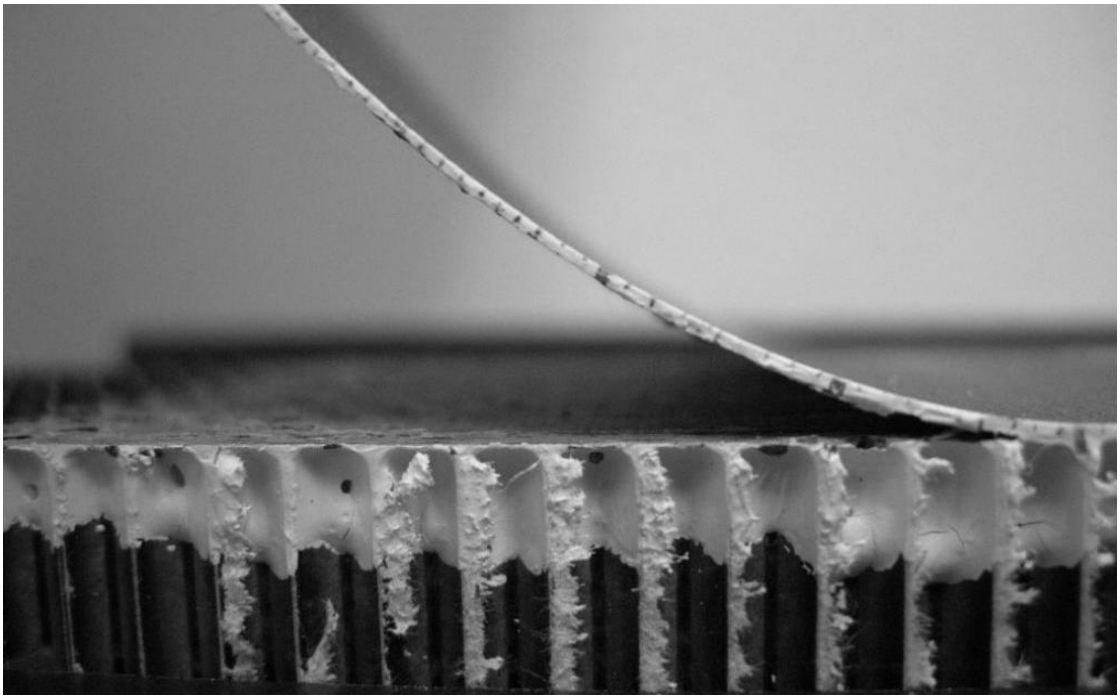

Figure 5-4: Overly complient untabbed facesheet debonding from core

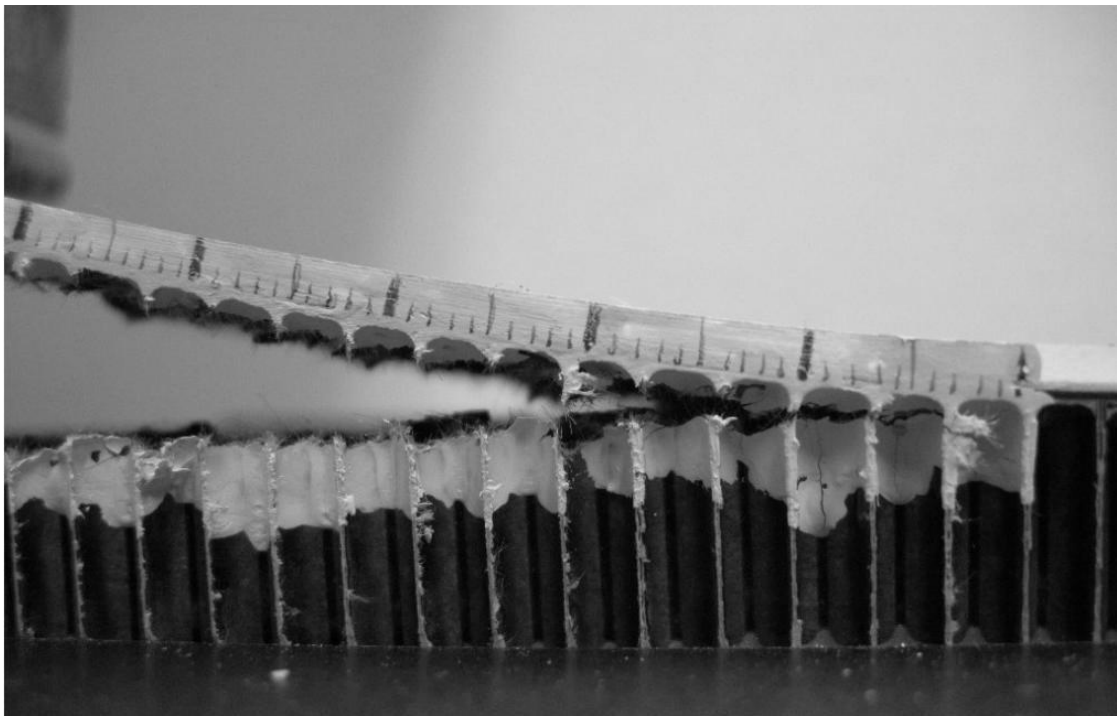

Figure 5-5: Thin facesheet specimen reinforced with 1.6 mm (0.063 in.) tabbing debonding from core.

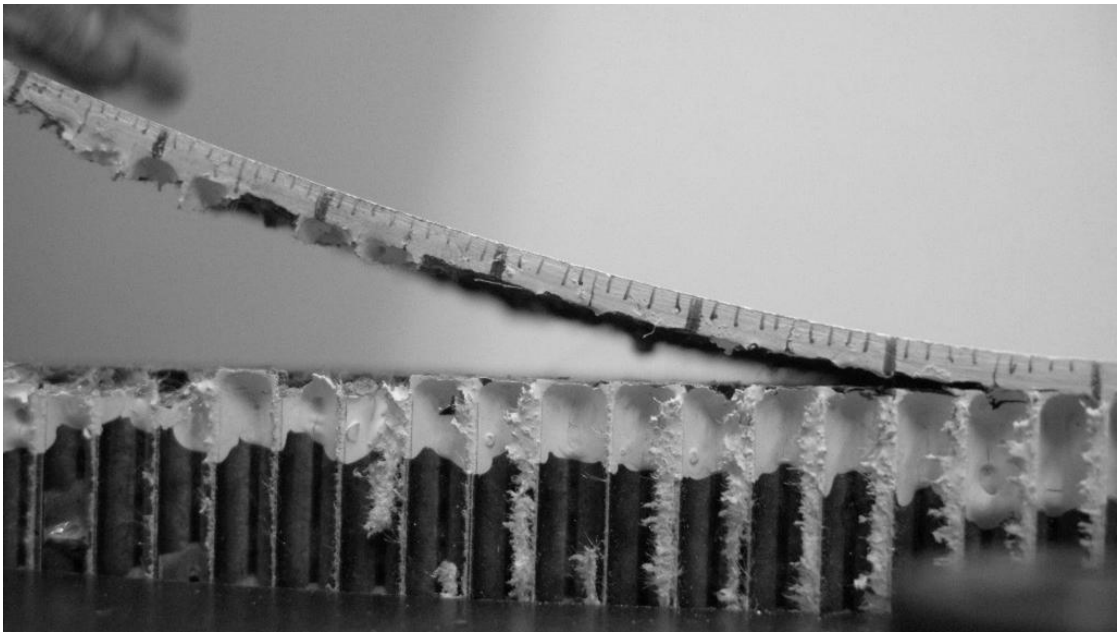

Figure 5-6: Thin facesheet specimen reinforced with 0.51 mm (0.02 in.) tabbing debonding from core

This difference in failure modes was not expected. The difference in failure location seen in the different coupon configurations is also reflected in their respective G_c measurements, as shown in Figure 5-7. The 1.6 mm (0.063 in.) tabbed G_c measurements are significantly higher (four times) than the untabbed specimen. It is believed that this is because the debond was growing through the Nomex core rather than at the interface. This also explains why there is more variability in the 1.6 mm (0.063 in.) tabbed G_c measurements; since debond was propagating through the Nomex core rather than at the interface and the number of cell walls the debond was required to overcome varied, as was discussed in Section 4.2. The untabbed specimen gave lower, yet more consistent G_c values than the tabbed specimen. The 0.51 mm (0.02 in.) tabbed specimen, which was seen to initially yield in the core, at the base of the adhesive fillets, and later to fail at the facesheet/core interface, resulted in G_c measurements, which initially were comparable to the 1.6 mm (0.063 in.) tabbed specimen and later comparable to the untabbed specimen.

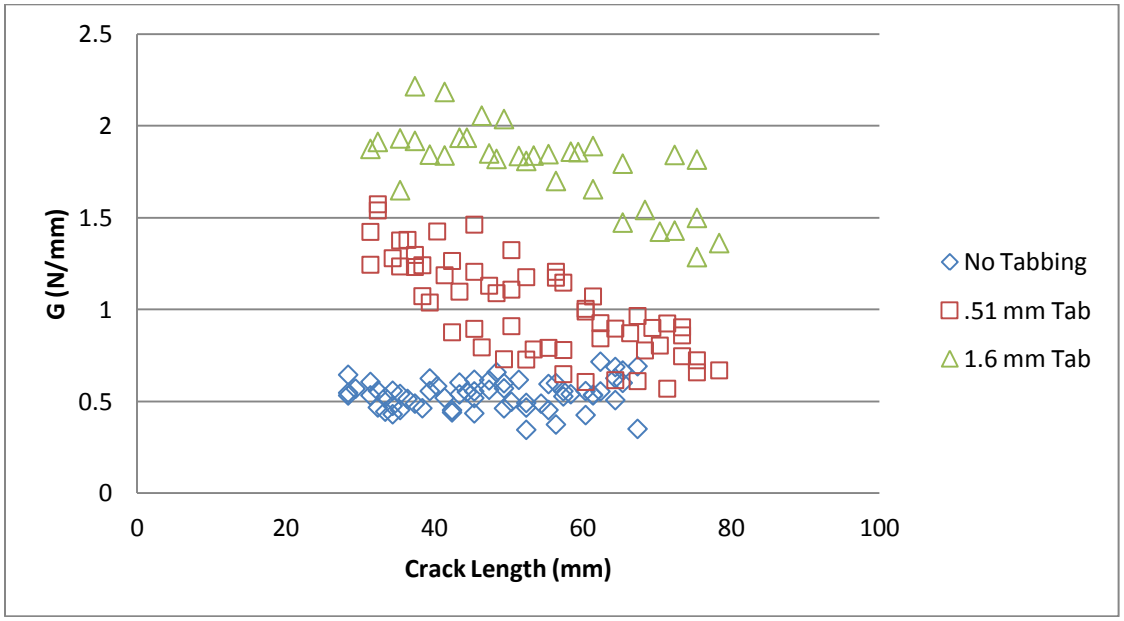

Figure 5-7: G_c vs. debond length for thin facesheeted sandwich constructions

Given that each of the test groups originated from the same parent panel, the bond integrity of the facesheet to the core was consistent for each of the test groups. The fact that the failure location and G_c measurements varied so widely during testing shows that the addition of the facesheet doubler did affect the outcome of the tests. It is believed that the addition of the doubler to the facesheet undergoing deflection is creating a more complex state of bending stresses. In a sense, the tabbed facesheet is being transformed to a thin, nonsymmetric sandwich composite beam itself; created by the G-10 tabbing, the epoxy and wires (used to gauge the bond line thickness) bonding the tabbing to the facesheet, and the upper facesheet. Capturing the stress profiles and interactions of the thin layers comprising the upper facesheet "structure" was found to be difficult as in depth analysis of the stress state near the debond front for tabbed and untabbed coupons showed the normal and shear stresses (at a constant G_c) to be similar. As well each case still showed very high (greater than 96%) Mode I dominated debond growth.

It is therefore believed that the addition of tabbing to the facesheet is not the best method to limit deflections, as the location of debond growth and G_c values were altered when the tabbing was added. In addition, previous research [6] related to the development of this test standard showed facesheet thickness not to affect G_c measurements, as seen in Figure 5-8. Along these same lines, research involving peel testing of flexible laminates and adhesive joints also showed no effect on G measurements due adherend thickness [21 and 22]. Lastly, the G_c values obtained during this testing of untabbed thin, three ply facesheet coupons agrees with G_c values obtained during the testing of thicker six Ply facesheeted Nomex coupons ; all of which measured a value of approximately 0.5 N/mm regardless of facesheet thickness or deflection.

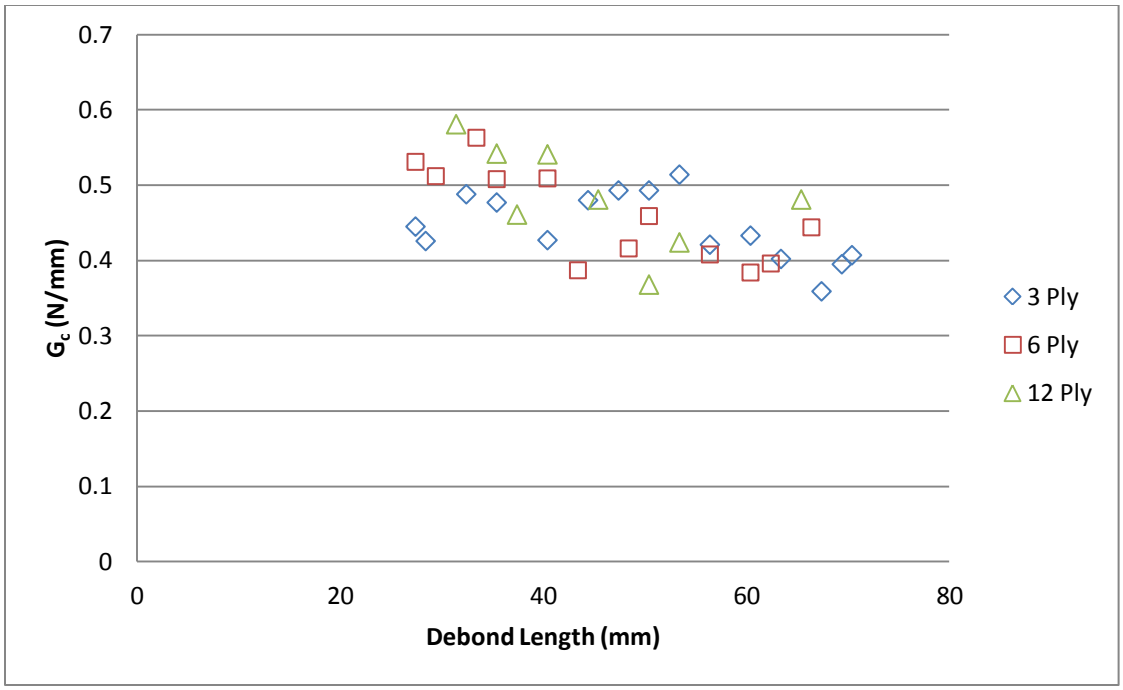

Figure 5-8: G_c data for coupons of different facesheet thickness

Although FEA showed that the addition of a facesheet doubler improved G_c agreement between thin facesheet sandwiches and their thicker facesheet counterparts, it was shown experimentally that the addition of facesheet doublers altered the location of debond propagation and resulted in inconsistent G_c measurements. For this reason the addition of doublers to thin facesheeted coupons is believed to be unnecessary and is discouraged due to the fact that the location of debond growth and the G_c measurements were altered. The change of failure location seen in the tabbed specimens is believed to be caused by the altering of the flexural modulus of the upper facesheet and the interactions between the core, tabbing, adhesive, and carbon fiber layers. It was shown through experimental testing that thin untabbed sandwiches, although they deflected more than 20% the length of the debond, measured similar G_c values to thicker facesheeted sandwiches that conform to the minimum deflection guideline.

6 EFFECT OF DEBOND LOCATION

The SCB test configuration was selected after detailed analysis and coupon testing showed that it provided the highest percentages of Mode I dominated crack growth [5 and 6]. As well, this test configuration localized the stresses in the core to the debond front and minimized crack kinking. However, the past analyses were performed under the assumption that debond propagation occurred directly at the facesheet/core interface, and the layer of adhesive used to bond the facesheet to the core was omitted from the FE model. Additionally, there was a concern that since previous analysis took place at the interface of two dissimilar materials, that the predicted mode mixity using VCCT may not be accurate.

To investigate whether or not the assumptions made in the previous analyses were valid, the FE model was modified to include the adhesive layer between the facesheet and core. The layer of film adhesive between the facesheet and core was modeled using two elements through the thickness of the adhesive layer. This allowed the user to more precisely specify the location of the debond and analyze the effects of including the adhesive layer in the FE model. This analysis entailed debond growth at five different locations; the core/adhesive interface, the facesheet/adhesive interface, within the adhesive layer, within the core (in the vicinity of the upper facesheet/core interface) and directly at the interface of the facesheet and core (completely omitting the adhesive layer), as shown in Figure 6-1 through Figure 6-5. The finite element model for this

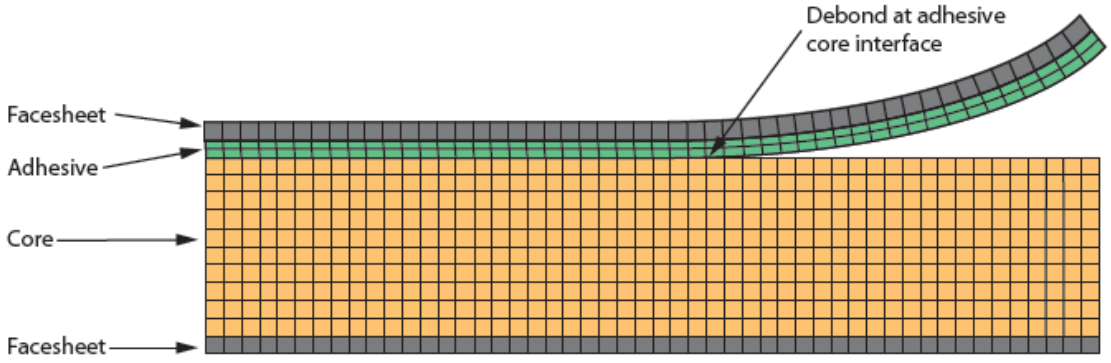

Figure 6-1. Debond growth at core/adhesive interface

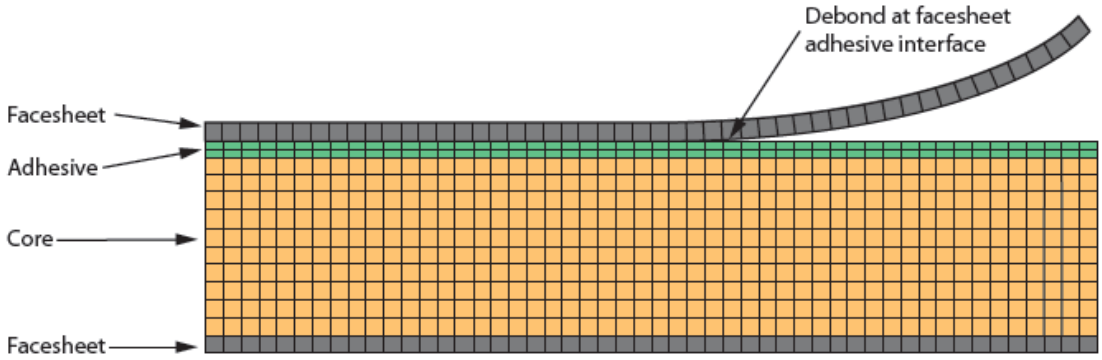

Figure 6-2. Debond growth at facesheet/adhesive interface

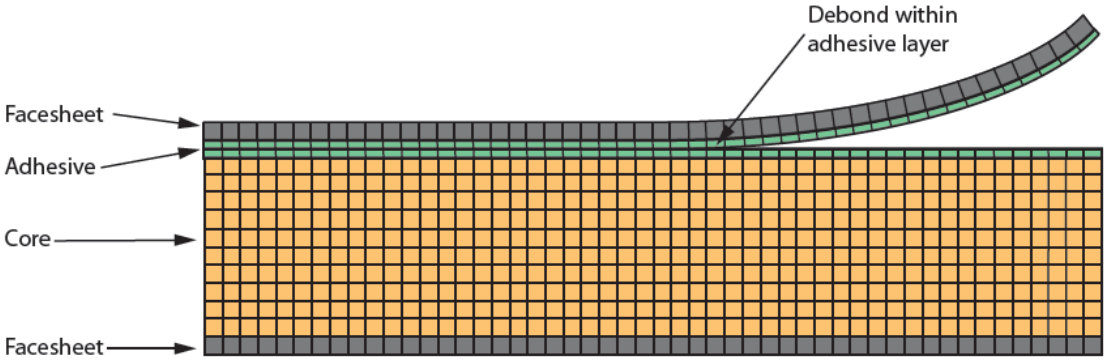

Figure 6-3. Debond growth within adhesive layer

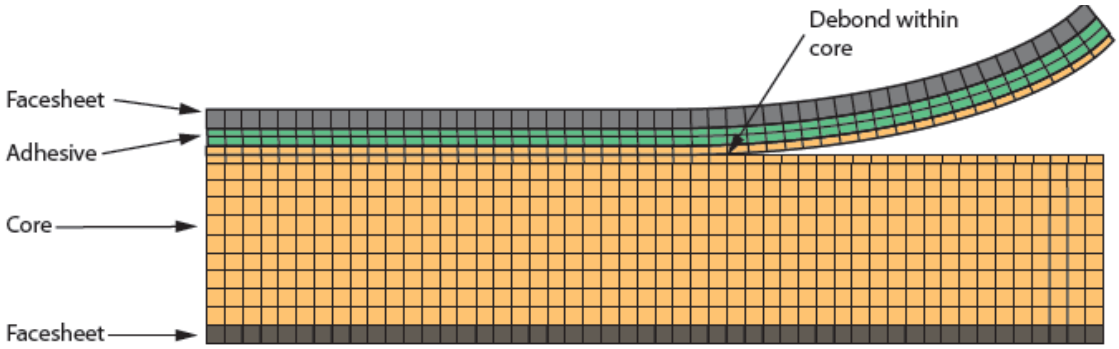

Figure 6-4: Debond growth within core, but still near the facesheet/core interface

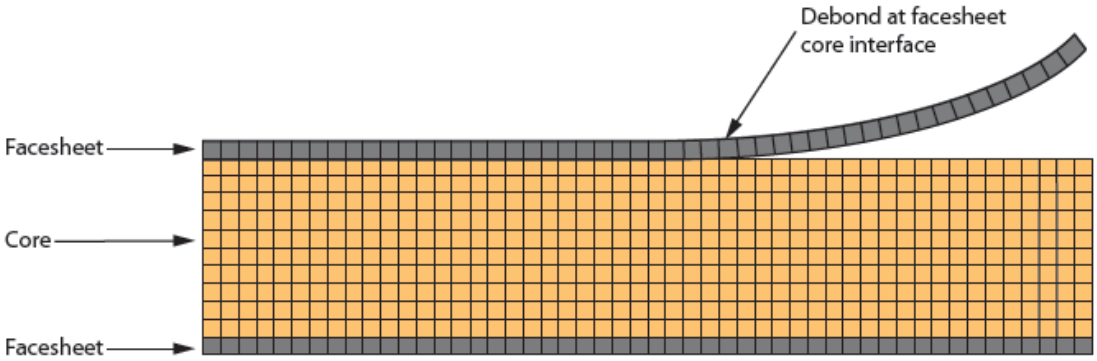

Figure 6-5: Debond growth at facesheet/core interface (adhesive omitted)

analysis used the same element size, mesh, and mesh density as was used during the test fixturing/mode mixity study described in Section 3.2, however, the aspect ratio of elements within the adhesive layer were half that of the elements used in the facesheets and core.

For each of the above configurations, it was found that the SCB arm undergoing deflection possessed slightly different compliances. This is due to the varying amount of material undergoing deformation for each configuration. For this reason, rather than performing analysis for each configuration at a constant load or constant deflection, the load inputs were adjusted in an iterative manner so as to achieve a constant G_c value. VCCT was then used to determine the mode mixity for each configuration at multiple debond lengths. As can be seen through inspection of these results, shown in Figure 6-6,

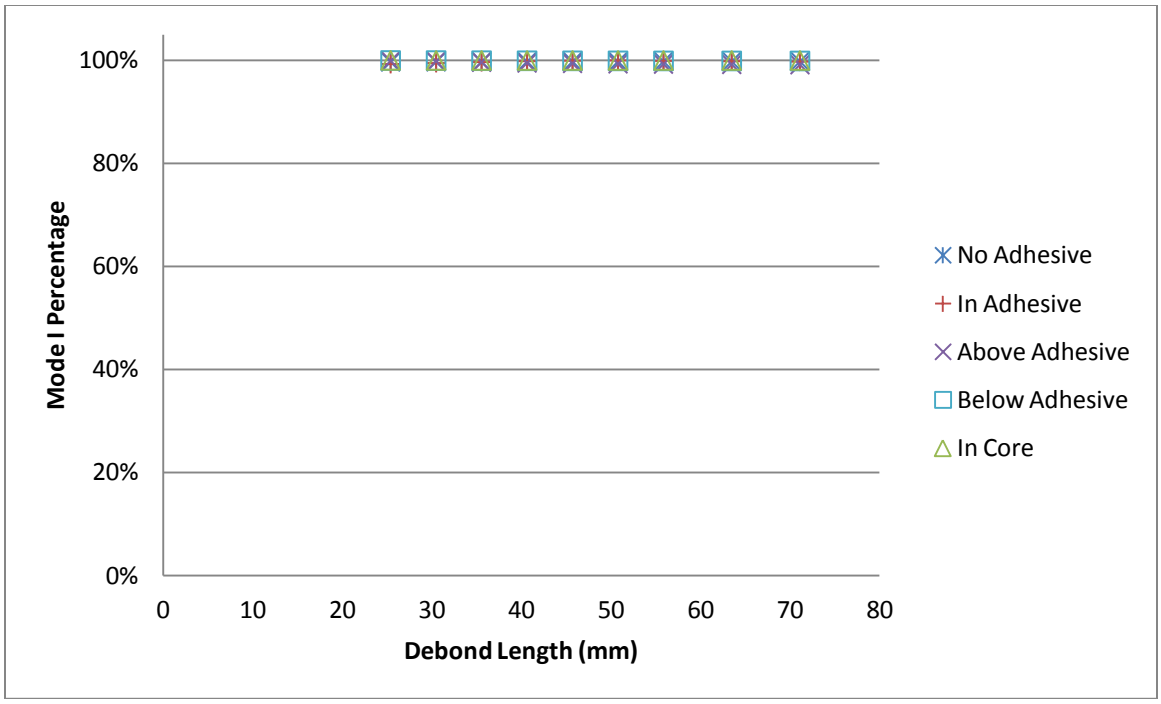

Figure 6-6: Mode mixity for foam sandwiches with debond growth occurring at different interfaces

at least 99% Mode I dominated debond growth was predicted in the foam core sandwich configurations regardless of debond location or length. The results for Nomex honeycomb core sandwich configurations were nearly identical to those for the foam core sandwich configurations, however mode mixity results dropped slightly from 99% to 98% Mode I for the sandwich configurations investigated.

Another concern related to the location of debond growth was whether or not the initial positioning of the debond would alter its direction of growth. This concern was addressed through a series of tests using specimen prepared with initial debonds located between the core and film adhesive and between the facesheet and film adhesive as was illustrated in Figure 6-1 and Figure 6-2, respectively. Test results showed that for both placements of the initial disbond, propagation occurred at the same through-the-thickness location and in a similar manner. As well, little change was seen in G_c measurements

when the results from the two placements of initial disbond were compared, as shown in Figure 6-7. The average G_c value for from specimens with the initial debond placed between the core and adhesive was 0.47 N/mm (2.68 lbf/in) versus 0.48 N/mm (2.74 lbf/in) from specimens with the initial debond placed between the facesheet and adhesive.

Additional testing was performed in which the initial debond was placed directly in the center of the core, away from either facesheet/core interface. Of interest was whether the debond would continue to propagate along the centerline of the core or migrate towards the top or bottom facesheet/core interface. These tests were performed on the same three facesheet configurations as were used in the facesheet thickness study discussed in Section 5.2, since during that study they were each observed to fail in locations.

The first facesheet configuration, as listed in Table 2-2, was a thin, three ply, $[0/90/0]_T$ facesheet without any doubler bonded to it. The second facesheet configuration

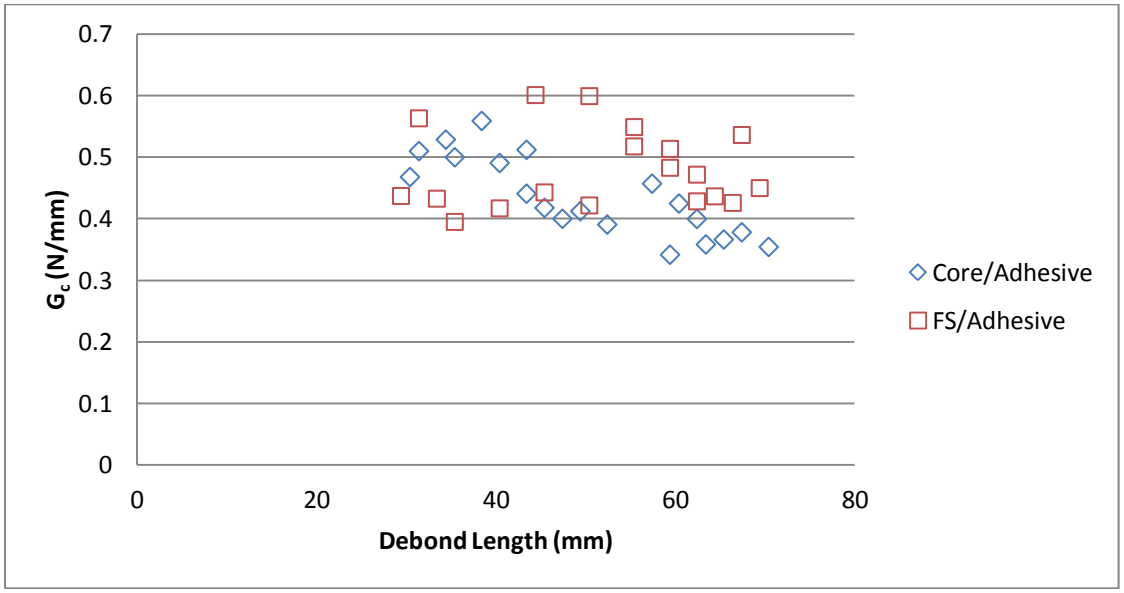

Figure 6-7: G_c measurements of Nomex specimen with initial debond at facesheet/adhesive interface and core/adhesive interface

incorporated the same three ply facesheet as the first configuration; however a 0.51 mm (0.02in.) thick G-10 doubler was bonded to the top of the facesheet. The third facesheet configuration was identical to the second configuration; however the thickness of the G-10 doubler was increased to 1.6 mm (0.063 in.). Two specimens of each configuration were tested.

The results of these tests are shown in Figure 6-8 through Figure 6-10. Results from all three sandwich configurations showed that as the debond propagated it began migrating towards the upper facesheet/core interface, resulting in a disbond in the vicinity of the facesheet/core interface. As described previously, however, a difference in the precise location of the disbond was noted as a function of facesheet stiffness: the thinner facesheet debonding along the facesheet/adhesive interface whereas the thicker tabbed facesheet debonding below the interface of the core and the film adhesive.

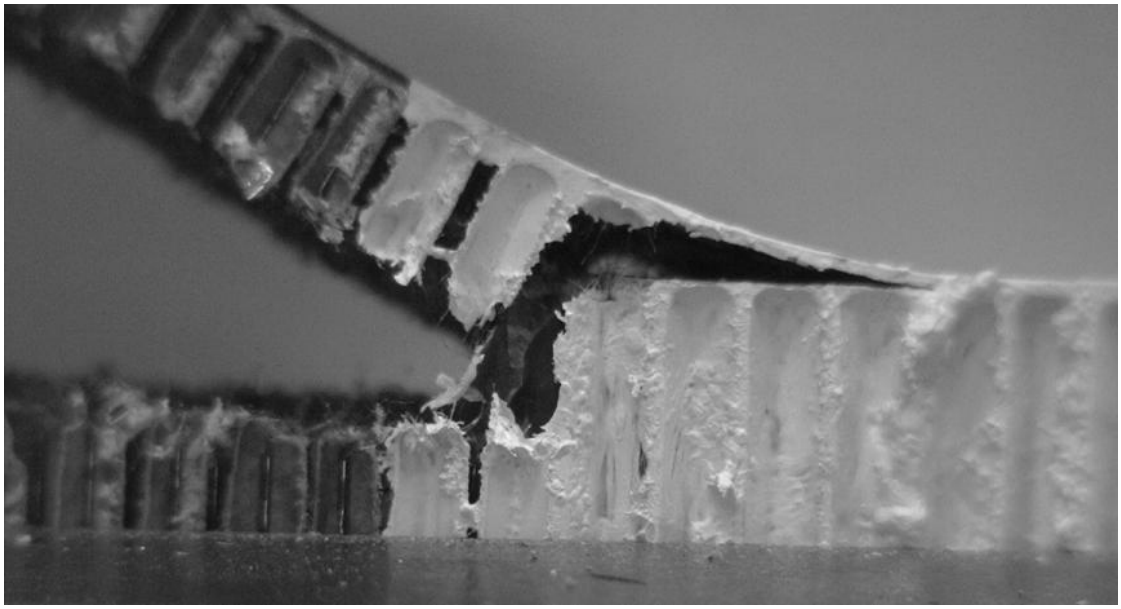

Figure 6-8 : Debond at center of core of un-tabbed thin facesheet coupon migrating to facesheet/core interface region

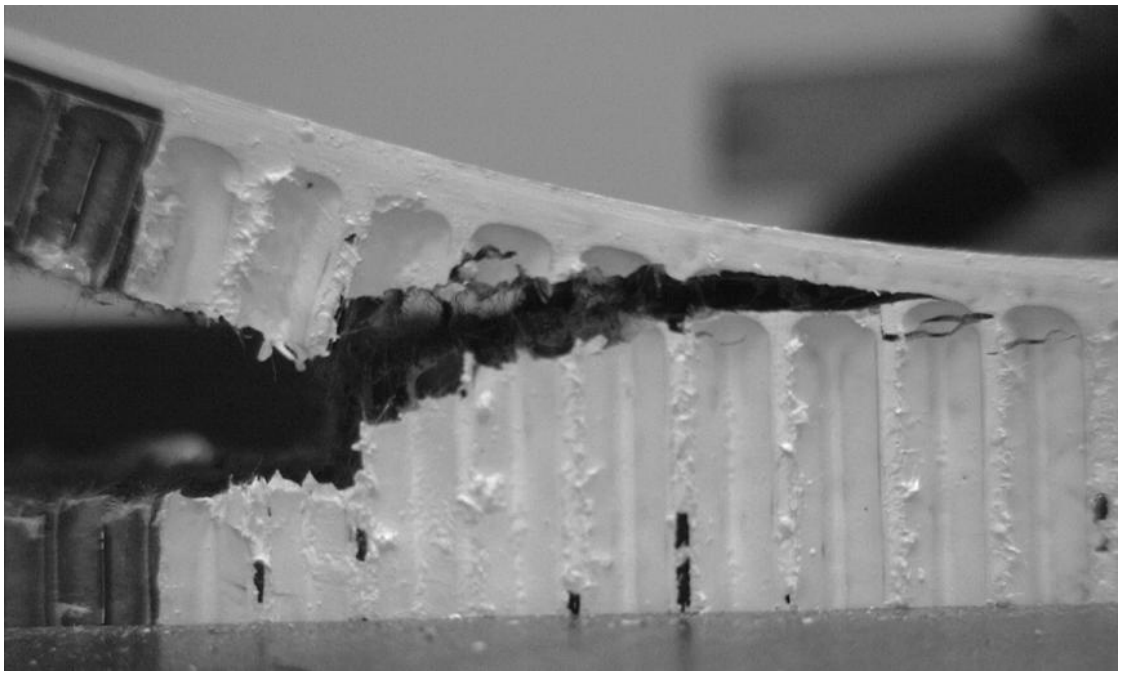

Figure 6-9: Debond at center of core of 0.51 mm (0.02 in.) tabbed specimen migrating to facesheet/core interface region

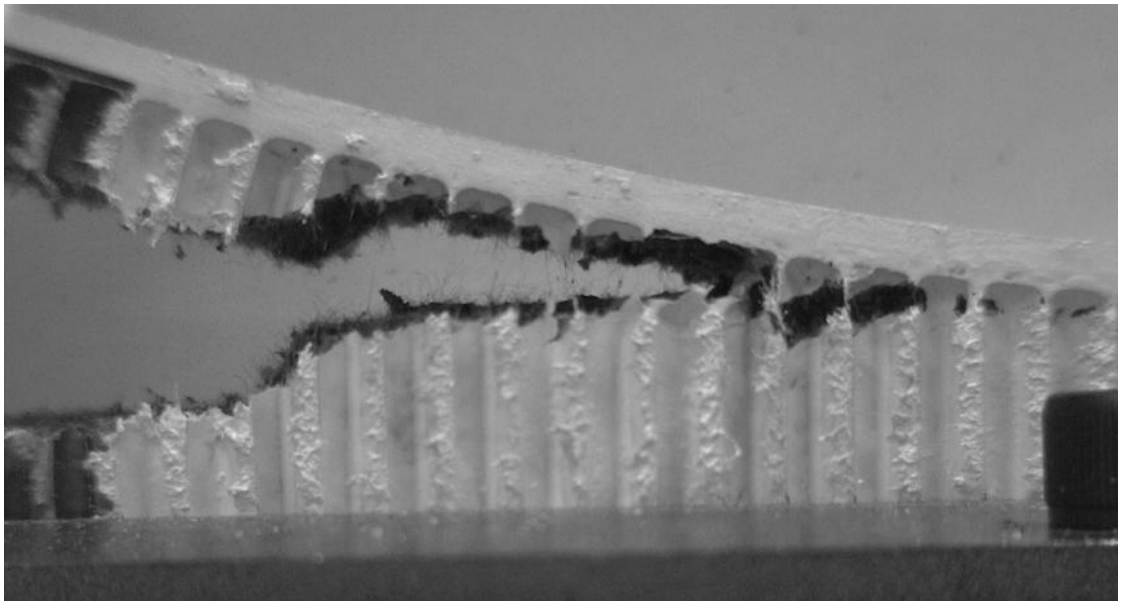

Figure 6-10: Debond at center of core of 1.6 mm (0.063 in.) tabbed specimen migrating to facesheet/core interface region

7 CONCLUSIONS

A Single Cantilever Beam (SCB) test fixture was designed and evaluated. Through the use of an edgewise clamping mechanism, testing could be performed in a laboratory environment quickly and efficiently. This fixture accommodates three specimen widths: 25.4 mm (1.0 in.), 50.8 mm (2.0 in.), and 76.2 mm (3.0 in.). The use of an elongated loading rod ensured that loading at the debond front maintained high Mode I dominance while the stationary base securely held the specimen in place, avoiding the possible inertial implications associated with the translating carriage base support.

It was determined that accurate G_c measurements required a minimum specimen width to ensure fully developed and self similar debond growth. Debond curvature was determined to be caused primarily by anticlastic curvature of the facesheet. Anticlastic curvature was dominant primarily in facesheets with high in-plane Poisson's ratio, such as quasi-isotropic layups. As well, for sandwich configurations with honeycomb cores, the number of honeycomb cells across the specimen width was found to affect the variability in G_c measurements. When too few cells were present across the width, increased scatter was seen due to the fluctuation in bond area as the debond propagated. For sandwich specimens with foam cores, a specimen width of 50.8 mm (2.0 in.) was found to be sufficient to generate consistent G_c measurements for all facesheet layups. For sandwich configurations with honeycomb cores, the same specimen width of 50.8 mm (2.0 in.) was seen to be sufficient. In addition to minimum width, however, it was

determined that at least six honeycomb cells are required across the width of the specimen. For this reason, when testing specimen with relatively large honeycomb cells, a greater specimen width may be required.

To investigate the effects of large facesheet rotations, which occurred when testing sandwich configurations with relatively thin, compliant facesheets, such sandwich configurations were also tested and analyzed with bonded facesheet doublers. The use of such facesheet doublers was proposed to limit facesheet deflections and rotations during SCB testing. Numerical simulations were performed following the Compliance Calibration method of data reduction along with the VCCT method. Finite element results suggested that the addition of bonded doublers to thin facesheet coupons could be used to reduce deflections. However, SCB testing showed that the addition of facesheet doublers altered the through-the-thickness location of disbond growth, thus affecting the resulting G_c results. Specimens with facesheet doublers were seen to fail in the core at the base of the adhesive fillets rather than directly along the facesheet/core interface, as was the case with specimens without facesheet doublers. Thus, although the addition of doublers to sandwich configurations with thin facesheets did reduce facesheet deflection and rotation, this practice was not found to be beneficial as failure locations were seen to change and conflicting G_c measurements were gathered.

An investigation into the effect of initial debond location was performed using both SCB testing and finite element analysis. SCB test results showed that regardless of the through-the-thickness placement of the initial disbond, crack growth migrated to the facesheet/core interface region. When the initial debond was positioned at the center of the core, the crack migrated from the center of the core to the facesheet/core interface

region. Finally, results from finite element analyses showed high Mode I dominance at the debond front, independent of the through-the-thickness location of the debond in the vicinity of the facesheet/core interface.

APPENDIX A

SANDWICH PANEL FABRICATION PROCEDURES

The fabrication of sandwich composites is a multistep process that is capable of producing stiff, light, high performance structures and components. However, if care is not taken throughout the entire layup and bonding processes, manufacturing defects can cause premature and unexpected failure of the structure, even though visually the structure appears to be sound. In the case of manufacturing sandwich panels used to build test coupons, manufacturing defects can lead to erroneous data, in turn skewing results, and possibly invalidating conclusions.

Foam Sandwich Panels

Vacuum Assisted Resin Transfer Molding (VARTM) was the process used to manufacture the foam core sandwich panels for this research. In this process, liquid resin is drawn into a sandwich panel inside a vacuum bag under vacuum. By layering release film and a mesh layer in the correct sequence, the resin is allowed to infiltrate the sandwich panel and cure, forming the facesheets and bonding them to the core in a single step. Shown in Figure A-1 is the stacking sequence used to provide a flow path for the resin, and allow successful infiltration.

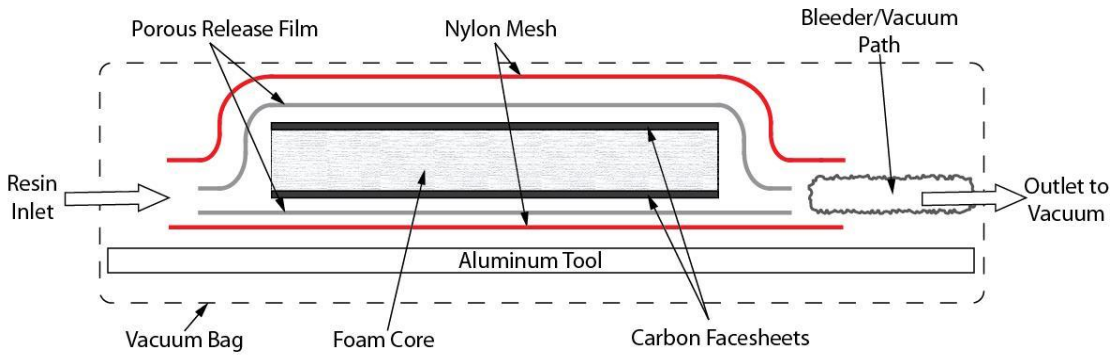

Figure A-1: Assembly used for VARTM process

Process:

1. Cut and orient the carbon fiber fabric layers in the desired stacking sequence for the facesheets on either side of the core. It is usually best to cut the carbon fiber layer slightly larger than the core so that the excess fabric can drape over the core, which aids in resin flow. Straight pins or thumb tacks can be used to secure the carbon fabric to the core to ensure that the layers do not shift during the assembly process.
2. On a tool plate covered with an adhesively-bonded nonporous Teflon coated fiberglass release layer, place a single layer of nylon mesh which allows a flow path between the tool and the sandwich panel. The dimensions of the mesh should be approximately 25 mm (2 in.) wider and 150 mm (6 in.) longer than the panel.
3. On top of the nylon mesh place one or two layers of porous Teflon coated fiberglass release film. This release film provides a high quality surface finish to the sandwich panel and allows the panel to be separated from the layer of nylon mesh following cure. The release film should be approximately the same dimensions as the nylon mesh.

4. Place the sandwich panel assembly onto the release film such that there is approximately a 25 mm (1 in.) border on either side of the panel and approximately a 25 - 51 mm (1 – 2 in.) border at the front of the panel. There will be approximately a 100 - 125 mm (4 – 5 in.) border along the rear edge of the panel, as shown in Figure A-2.
5. Cut and fold a piece of felt bleeder material into a bundle so that it is approximately as wide as the sandwich panel and place it on the layer of release film and mesh about 25 mm (1in.) from the rear edge of the panel, as shown in Figure A-2. This bleeder will serve to both absorb excess resin and to provide a vacuum path. The folded bleeder bundle should be at least four layers of felt thick.

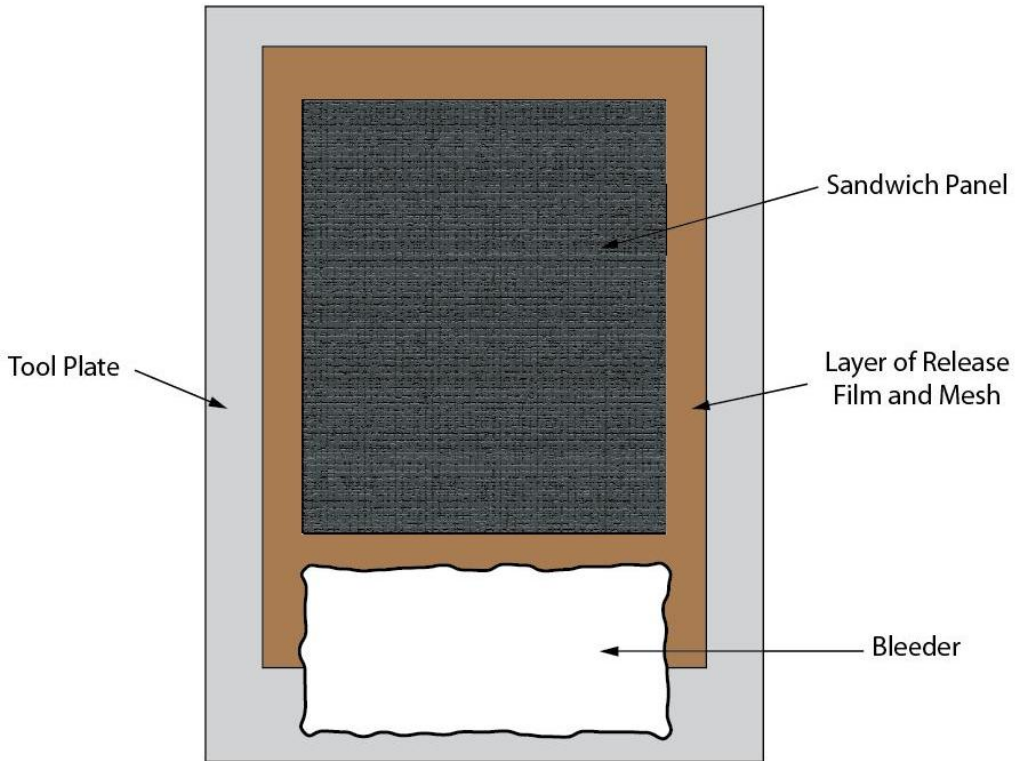

Figure A-2: Top view of VARTM layup showing borders of sandwich panel, bleeder, release film and mesh

6. On top of the sandwich panel and bleeder cloth, place another layer of porous Teflon coated fiberglass release film.
7. Place another layer of nylon mesh on top of the release film
8. Place the entire assembly inside a vacuum bag.
    a. Prior to sealing the vacuum bag, place a vacuum tube in the end of the assembly containing the bleeder cloth, making sure the end of the tube is inserted only 25 mm (1 in.) into the layers of bleeder cloth. The bleeder cloth is used not only as a vacuum path, but also to absorb excess resin during the infiltration process. If the vacuum tube is inserted too far into the bleeder cloth, resin may be pulled into the vacuum tube, clogging the tube and possibly damaging the vacuum pump.
    b. At the opposite end of the vacuum bag, insert a separate tube which will act as a siphoning tube for inputting the resin. Ensure that the end of the siphoning tube is layered between the top and bottom layers of the release film and mesh to allow a flow path for the resin. To aid in distributing resin and to create a more even resin flow, the siphoning tube can be bent into an L-shape and holes cut into the side walls, creating multiple "resin ports" as shown in Figure A-3. Place a tube clamp on the siphoning tube for controlling the resin flow rate into the vacuum bag.
9. Seal both ends of the bag and turn on the vacuum pump.
10. Place the free end of the siphon tube into the container containing the resin and slowly open the tube clamp, allowing the resin to flow into the vacuum bag. Once resin begins to flow through the tube, keep the siphoning tube in the resin to

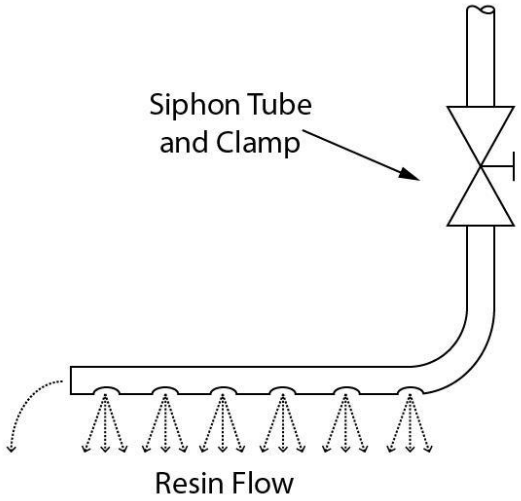

Figure A-3: Improved distribution of resin through siphoning tube

prevent air bubbles from being pulled into the panel. Adjust the resin flow rate using the siphon tube clamp so that the resin is pulled across the sandwich panel evenly. Once the resin has completely infiltrated the panel, completely close the clamp and allow the resin to cure under vacuum.

Nomex Honeycomb Panels

A two-step process was used to manufacture the Nomex honeycomb core sandwich panels used in this research. First the facesheets were fabricated from unidirectional carbon/epoxy fiber prepreg. Second, the facesheets were bonded to the honeycomb core in a secondary bonding operation using film adhesive. Two manufacturing techniques were used to fabricate the facesheets: press curing and autoclave curing.

Press Curing

In press curing, the pressure and heat required to cure the carbon/epoxy prepreg is supplied by a hydraulic press with heated platens. A flat 305 x 305 mm (12 x 12 in.)

well-and-plunger style mold with removable sides was used to enclose the prepreg and control its shape and surface flatness, as shown in Figure A-4.

Process

1. Cover all surfaces of the mold that will be in contact with the carbon/epoxy prepreg with an adhesively-bonded nonporous Teflon coated fiberglass release layer. Clean the threaded surfaces of the fasteners/holes used to clamp the mold edges to the base plate and apply a spray release agent. Loosely attach the mold sides to the base, leaving a small gap between the side and mold base. Confirm that there are no tears, wrinkles, or blemishes in the tool release layer which may affect the surface finish of the cured facesheets.
2. Cut and lay-up the carbon/epoxy prepreg into the desired facesheet stacking sequence. The dimensions of the facesheets should be the same as the inner dimensions of the mold.
3. Cut and place a layer of porous Teflon-coated fiberglass release film in the bottom of the mold.

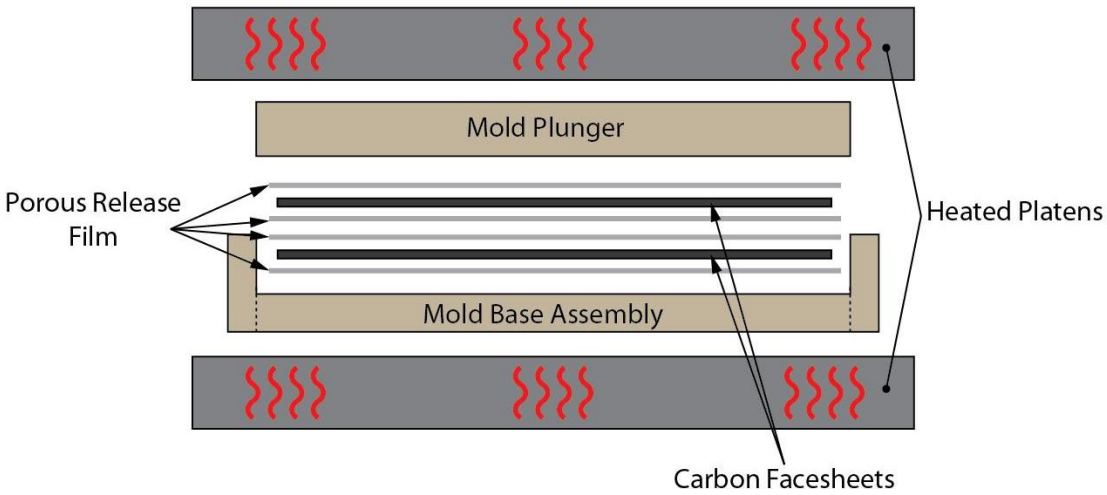

Figure A-4: Fabrication of press-cured facesheets

4. Place the uncured facesheet material into the mold.
5. If fabricating more than one facesheet laminates, place two layers of release film between adjacent laminates and a single layer between the top laminate and the plunger, as shown in Figure A-4. If making a single laminate only one layer of release film is required at the top of the laminate.
6. Carefully place plunger into the mold.
7. Tighten the fasteners securing the mold sides.
8. Place entire mold assembly into the press and follow the prepreg manufacturer's recommended cure cycle.

Autoclave Curing

An autoclave can be used to provide the heat and pressure needed to fabricate the laminates following the layering sequence shown in Figure A-5.

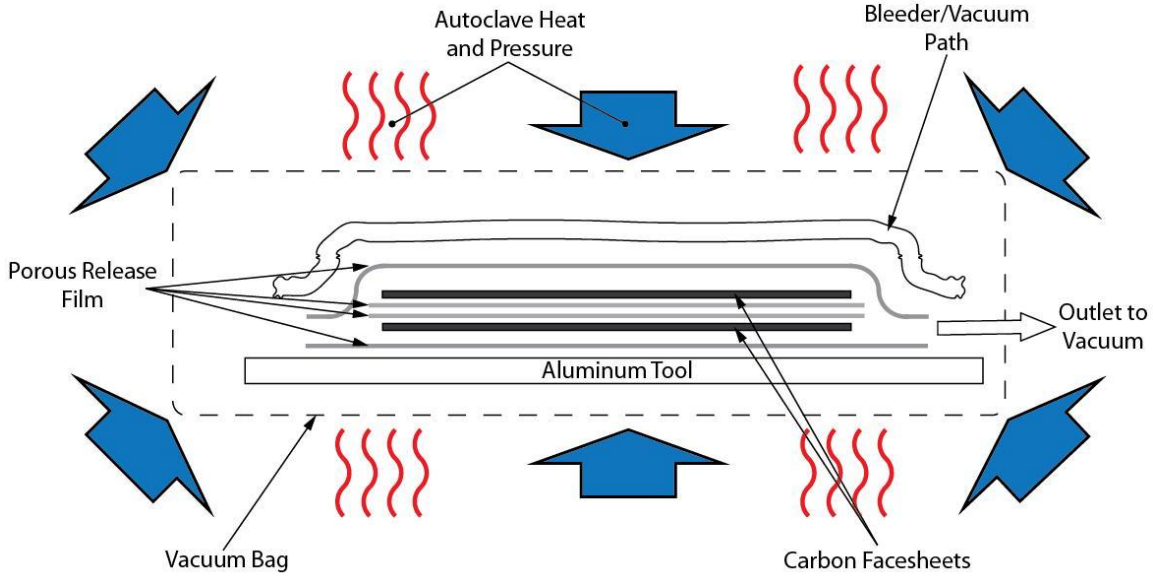

Figure A-5: Layering sequence for curing laminates in an autoclave

Process

1. Cut out and lay up the carbon fiber prepreg into the desired stacking sequence.
2. On a flat tooling plate covered with an adhesively-bonded nonporous Teflon coated fiberglass release layer, place a single layer of porous Teflon-coated fiberglass release film. The dimensions of the release film should be at least 6 mm (0.25 in.) larger than the laminate's length and width.
3. Center the uncured facesheet laminate onto the release film. Continue to layer additional facesheet laminates and release film, ensuring that there are two plies of release film between adjacent laminates, as shown in Figure A-5.
4. On the top facesheet laminate, place a single layer of release film followed by a layer of bleeder/breather material to provide a vacuum path and absorb excess resin.
5. Place the entire assembly into a vacuum bag.
6. Prior to sealing the vacuum bag, place a vacuum tube into the bag and ensure that it is inserted a sufficient distance to contact the bleeder/breather material and provide an adequate vacuum path.
7. Seal the vacuum bag and apply a vacuum.
8. Insert the entire vacuum bag assembly into the autoclave, making sure to protect the bag from punctures.
9. Cure the facesheet laminates in the autoclave following the prepreg manufacturer's recommended cure cycle.

Bonding of Facesheets to the Core

A secondary bonding operation may be performed to adhesively bond pre-cured composite facesheets to a honeycomb core with a film adhesive as shown in Figure A-6.

Process

1. Using intermediate grit sandpaper, abrade the bonding surface of both facesheets. Take care not to sand too deep into the surface of the laminate and damage the carbon fibers.
2. Clean the abraded surface of the laminate with acetone and wipe clean. Repeat until all residue and contaminants are removed from the surface. Care should be taken not to touch the bond surface of the laminate once clean, as the oils from hands will contaminate the bond surface.
3. Place a layer of film adhesive on the abraded and cleaned surface of the laminates, and set onto either surface of the core. When using Nomex honeycomb, it is not necessary to clean the surface of the core if free of debris and oil. If using an aluminum core, a more extensive acid etching process may be required to prep the surface for bonding.
4. Place the panel assembly onto the tooling plate, covered with an adhesively-bonded nonporous Teflon coated fiberglass release layer and an additional layer of release film as shown in Figure A-6.
5. Place an additional layer of release film on the top of the panel assembly, making sure that the dimensions of this top release layer are adequate to drape over the edges and cover the sides of the panel.

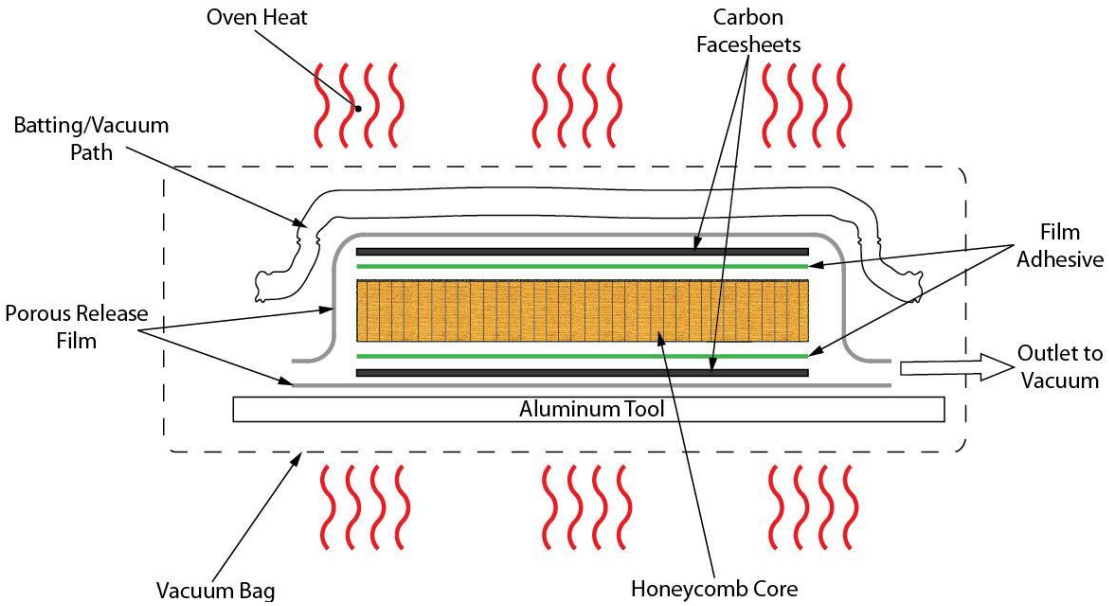

Figure A-6: Bonding of facesheets to core through secondary bond process

6. Place a layer of bleeder/breather material on top of the assembly to provide a vacuum path.
7. Insert the assembly into a vacuum bag. Prior to sealing, place a vacuum tube into the bag and ensure that it is inserted a sufficient distance to contact the bleeder/breather material and provide an adequate vacuum path.
8. Seal the vacuum bag and apply a vacuum.
9. Insert the entire vacuum bag assembly into the autoclave, making sure to protect the bag from punctures.
10. Cure the film adhesive in the autoclave following the film adhesive manufacturer's recommended cure cycle.

To prevent edgewise crushing of the lower density honeycomb cores when subjected to vacuum, the open edges of the assembled sandwich panel were covered with high-temperature tape, as shown in Figure A-7. The application of the tape was

determined to be sufficient to prevent the edges of the core from crushing while not interfering with the compaction of the facesheet onto the core.

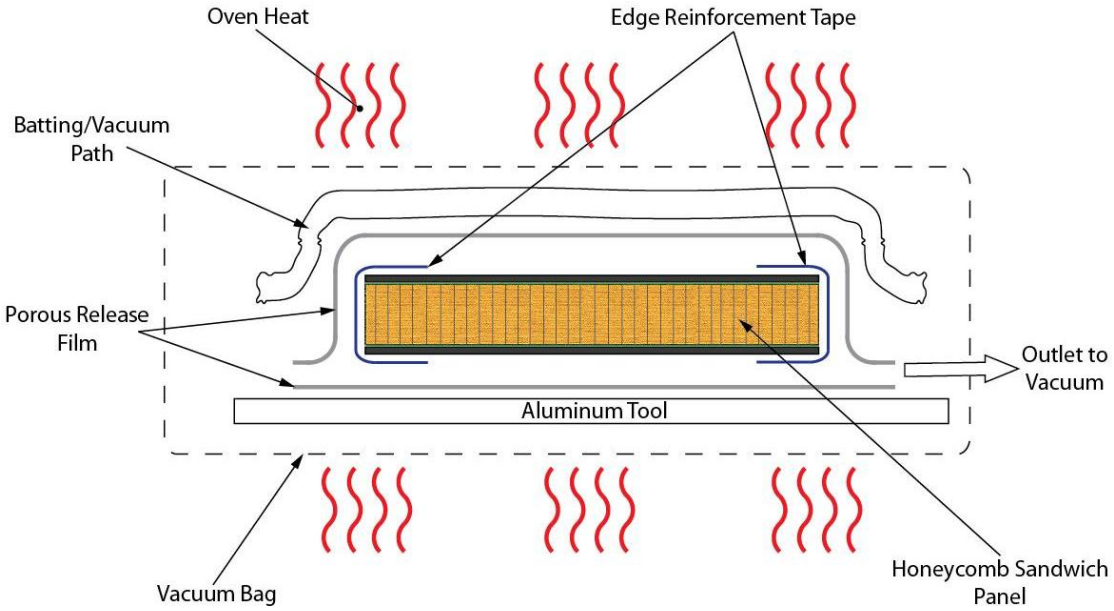

Figure A-7: Preventing edgewise crushing of low density honeycomb cores through use of taped panel edges

APPENDIX B

DRAFT TEST STANDARD: SINGLE CANTILEVER BEAM (SCB) TEST

Standard Test Method for

Mode I Interface Fracture Toughness of Sandwich Constructions

1. Scope

1.1 This test method describes the determination of the opening Mode I fracture toughness, G_{Ic}, of the core-to facing interface of an assembled sandwich panel using the single cantilever beam (SCB) specimen.

1.2 This test method is limited to use with sandwich composites consisting of facings bonded to a core. Permissible core material forms include those with continuous bonding surfaces (such as balsa wood and foams) as well as those with discontinuous bonding surfaces (such as honeycomb). This test method may prove useful for other types and classes of sandwich constructions however, certain interferences have been noted (see 6.5).

1.3 The values stated in SI units are to be regarded as the standard. The values given in parentheses are for information only.

1.4 This standard may involve hazardous materials, operations, and equipment.

1.5 *This standard does not purport to address all of the safety concerns, if any, associated with its use. It is the responsibility of the user of this standard to establish*

appropriate safety and health practices and determine the applicability of regulatory limitations prior to use.

2. Referenced Documents

2.1 *ASTM Standards:*

C274 Terminology of Structural Sandwich Construction

D883 Terminology Relating to Plastics

D5528 Mode I Interlaminar Fracture Toughness of Unidirectional Fiber-Reinforced Polymer Matrix Composites

D2651 Guide for Preparation of Metal Surfaces for Adhesive Bonding

D2734 Test Methods for Void Content of Reinforced Plastics

D3171 Test Methods for Constituent Content of Composite Materials

D3878 Terminology for Composite Materials

D5229/D 5229M Test Method for Moisture Absorption Properties and Equilibrium Conditioning of Polymer Matrix Composite Materials

E4 Practices for Force Verification of Testing Machines

E6 Terminology Relating to Methods of Mechanical Testing

E122 Practice for Calculating Sample Size to Estimate, With Specified Precision, the Average for a Characteristic of a Lot or Process

E177 Practice for Use of the Terms Precision and Bias in ASTM Test Methods

E456 Terminology Relating to Quality and Statistics

E691 Practice for Conducting an Interlaboratory Study to Determine the Precision of a Test Method

E1471 Guide for Identification of Fibers, Fillers, and Core Materials in Computerized Material Property Databases

3. Terminology

3.1 Terminology D3878 defines terms relating to high-modulus fibers and their composites. Terminology C274 defines terms relating to structural sandwich constructions. Terminology D883 defines terms relating to plastics. Terminology E6 defines terms relating to mechanical testing. Terminology E456 and Practice E177 define terms relating to statistics. In the event of conflict between terms, Terminology D3878 shall have precedence over the other terminology standards.

3.2 *Definitions of Terms Specific to This Standard:*

3.2.1 *crack opening mode (Mode I)*—fracture mode in which the delamination faces open away from each other.

3.2.2 *Mode I interlaminar fracture toughness, G_{Ic}*—the critical value of *G* for delamination growth as a result of an opening load or displacement.

3.2.3 *energy release rate, G*—the loss of energy, dU, in the test specimen per unit of specimen width for an infinitesimal increase in delamination length, *da*, for a delamination growing under a constant displacement. In mathematical form,

$$G = -\frac{1}{b}\frac{dU}{da} \qquad (1)$$

where:

U = total elastic energy in the test specimen,

b = specimen width, and

a = delamination length.

3.3 Symbols

3.3.1 A_1—slope of plot of a/b versus $C^{1/3}$.

3.3.2 a—delamination length.

3.3.3 a_0—initial delamination length.

3.3.4 b—width of DCB specimen.

3.3.5 C—compliance, δ/P, of DCB specimen.

3.3.6 CV—coefficient of variation, %.

3.3.7 da—differential increase in delamination length.

3.3.8 dU—differential increase in strain energy.

3.3.9 E_{11}—modulus of elasticity in the fiber direction.

3.3.10 E_{1f}—modulus of elasticity in the fiber direction measured in flexure.

3.3.11 F—large displacement correction factor.

3.3.12 G—strain energy release rate.

3.3.13 G_{Ic}— opening Mode I interlaminar fracture toughness.

3.3.14 h—thickness of DCB specimen.

3.3.15 L—length of DCB specimen.

3.3.16 L'—half width of loading block.

3.3.17 m—number of plies in DCB specimen.

3.3.18 N—loading block correction factor.

3.3.19 *NL*—point at which the load versus opening displacement curve becomes nonlinear.

3.3.20 *n*—slope of plot of Log C versus Log a.

3.3.21 *P*—applied load.

3.3.22 P_{max}— maximum applied load during DCB test.

3.3.23 *SD*—standard deviation.

3.3.24 *t*—distance from loading block pin to center line of top specimen arm.

3.3.25 *U*—strain energy.

3.3.26 *VIS*—point at which delamination is observed visually on specimen edge.

3.3.27 V_f— fiber volume fraction, %.

3.3.28 δ—load point deflection.

3.3.29 Δ—effective delamination extension to correct for rotation of DCB arms at delamination front.

3.3.30 Δ_x—incremental change in Log a.

3.3.31 Δ_y—incremental change in Log C.

4. Summary of Test Method

4.1 The SCB specimen shown in Figure B-1 consists of a sandwich construction containing a non-adhesive insert at one sandwich facing/core interface that serves as a disbond initiator. Opening forces are applied to the SCB specimen by means of a hinge (Figure B-1a) or loading block (Figure B-1b) bonded to one of the sandwich facings with the opposing facing fixed to the base of the test fixture. The end of the SCB specimen is opened by controlling either the opening displacement or the crosshead movement, while the load and disbond length are recorded.

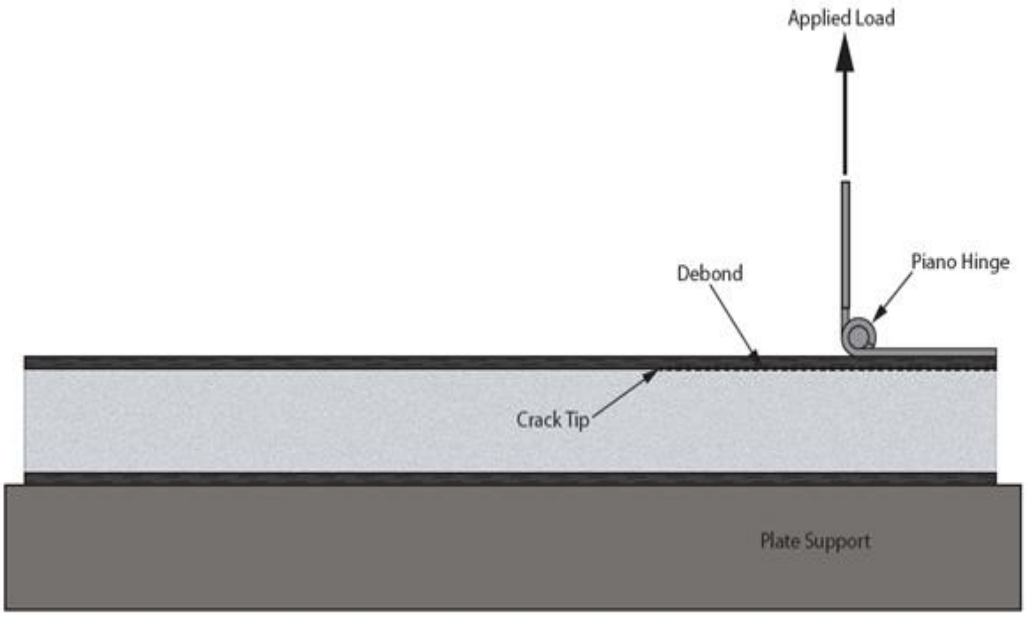

(a)

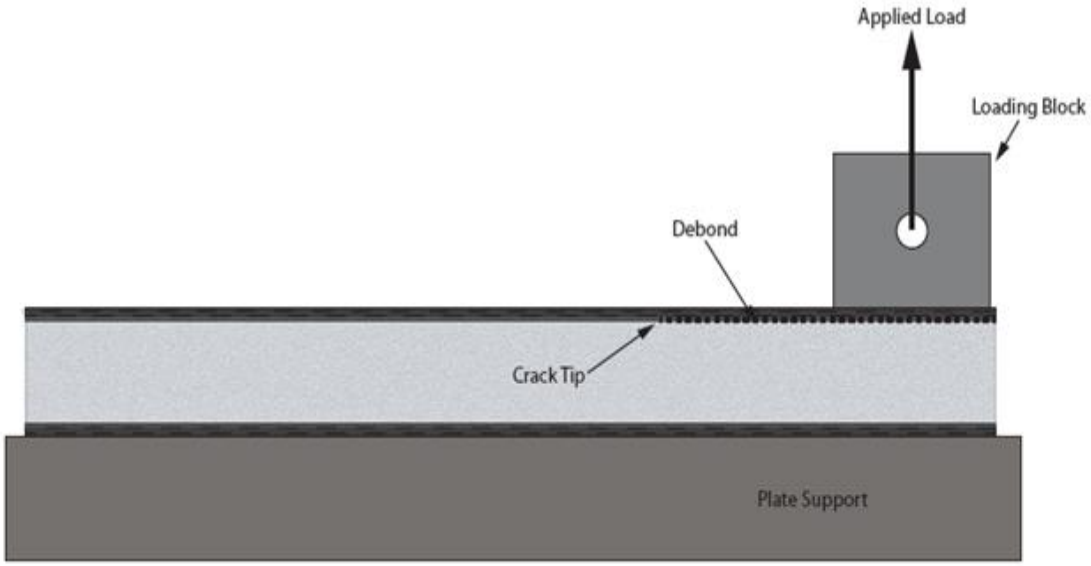

(b)

Figure B-1: Load application using (a) a hinge and (b) a loading block

4.2 The only acceptable failure modes for G_{Ic} are those resulting in disbond growth occurring either at, or in the vicinity of the core-to-facing interface, parallel to the plane of the interface.

4.3 A record of the applied load versus opening displacement is recorded on an *X-Y* recorder or equivalent real-time plotting device or stored digitally and postprocessed. Instantaneous delamination front locations are marked on the chart at intervals of delamination growth. The Mode I interface fracture toughness is calculated using a modified beam theory or compliance calibration method.

5. Significance and Use

5.1 In a sandwich panel, core-to-facing bond integrity is necessary to maintain facing stability and permit load transfer between the facings and core. Knowledge of a sandwich composite's resistance to interface fracture is useful for product development and material selection. Furthermore, a measurement of the Mode I interface fracture toughness, independent of specimen geometry or method of load introduction, is useful for establishing design allowables used in damage tolerance analyses of sandwich composite structures made from these materials.

5.2 Factors that influence the fracture toughness of the core-to-facing interface and shall therefore be reported include the following: core material and geometry (cell size), adhesive material, core density, adhesive thickness, specimen geometry, specimen preparation, specimen conditioning, adhesive void content.

5.3 This test method can serve the following purposes:

5.3.1 To compare quantitatively the relative values of G_{Ic} for sandwich composite materials with different constituents.

5.3.2 To develop delamination failure criteria for sandwich composite damage tolerance and durability analyses.

6. Interferences

6.1 Linear elastic behavior is assumed in the calculation of *G* used in this test method. This assumption is valid when the zone of damage or nonlinear deformation at the delamination front, or both, is small relative to the smallest specimen dimension, which is typically the thickness of the debonded facesheet.

6.2 *Material and Specimen Preparation* – Poor material fabrication practices, lack of control of fiber alignment and damage induced by improper specimen machining are known causes of high data scatter in composites in general. Important aspects of sandwich panel specimen preparation that contribute to data scatter are incomplete or non-uniform core bonding to facings, misalignment of core and facing elements, the existence of voids or other core and facing discontinuities, out of plane curvature, facing thickness variation and poor bond surface preparation. Lack of attention to these details can lead to high variability in test results.

6.3 The definition for an initiation value of G_{Ic} is the point at which disbond growth is visually observed on the edge (VIS) measured with a microscope as specified in 7.5.

6.4 Disbond growth may proceed in one of two ways: (1) by a slow stable extension or (2) a run-arrest extension in which the disbond front jumps ahead abruptly. The first type of growth is preferred, however a run-arrest extension type of disbond growth, as is typical with some sandwich configurations, is permitted. An unstable jump from the insert may be an indication of a problem with the insert. For example, the insert may not be completely disbonded from the laminate, or may be too thick, resulting in a large neat

resin pocket, or may contain a tear or fold. Furthermore, rapid disbond growth may introduce dynamic effects in both the test specimen and in the fracture morphology. Treatment and interpretation of these effects is beyond the scope of this test method. The first propagation G_{Ic} value is referred to as the Mode I precrack G_{Ic} and is not included with the G_{Ic} values obtained during the test.

6.5 *Application to Other Materials, Layups, and Architectures*:

6.5.1 Although the loading conditions at the disbond front are likely to be Mode I dominated, a mismatch in modulus between the facing and the core surrounding the disbond act to couple the normal and shear deformations ahead of the disbond, resulting in loading that is not pure Mode I. In addition, composite facings with high in-plane Poisson's properties, such as quasi-isotropic layups, may experience significant anticlastic bending effects that result in nonuniform delamination growth along the specimen width, particularly affecting the observed initiation values. These edge effects are increased when more compliant facings are used, due to the increased deflections required to produce disbond growth.

6.6 Large Displacements – Thin facings on sandwich panels will result in large deflections of the load point. In accordance with small displacement assumptions used in beam theory, load point displacements should be minimized as much as possible to ensure accurate G_{Ic} values are calculated.

7. Apparatus

7.1 *Testing Machine* — A properly calibrated test machine shall be used that can be operated in a displacement control mode with a constant displacement rate in the range

from 0.5 to 5.0 mm/min (0.02 to 0.20 in./min). The testing machine shall conform to the requirements of Practices E4 and shall satisfy the following requirements.

7.1.1 *Testing Machine Heads* – The testing machine shall have both an essentially stationary head or base and a moveable head.

7.1.2 *Load Indicator* — The testing machine load-sensing device shall be capable of indicating the total load carried by the test specimen. This device shall be essentially free from inertia lag at the specified rate of testing and shall indicate the load with an accuracy over the load range(s) of interest of within ±1 % of the indicated value.

7.1.3 *Fixturing* – The fixture used shall be a loading rod and base plate clamping assembly shown schematically in Figure B-2. The loading rod is connected to the piano hinge or pinned to the loading block bonded to the specimen on one end while the other end is connected to the crosshead of the test machine. The purpose of offsetting the load application point is to ensure that loading remains essentially vertical during testing, thus preventing the accumulation of shear deformation in the core which could introduce an unwanted mode II component of loading along the delamination front. The base plate contains a clamping mechanism to apply a clamping force to the sides of the lower facing, holding the specimen stationary during testing.

7.1.4 *Attachments to Testing Machine* – The testing machine heads shall be capable of being attached to the loading rod and the base plate assembly. The loading rod must be attached to the crosshead via a pinned connection thus preventing development of a moment arm in the rod.

7.2 *Opening Displacement Indicator*— The opening displacement may be estimated as the crosshead separation, provided the deformation of the testing machine, with the

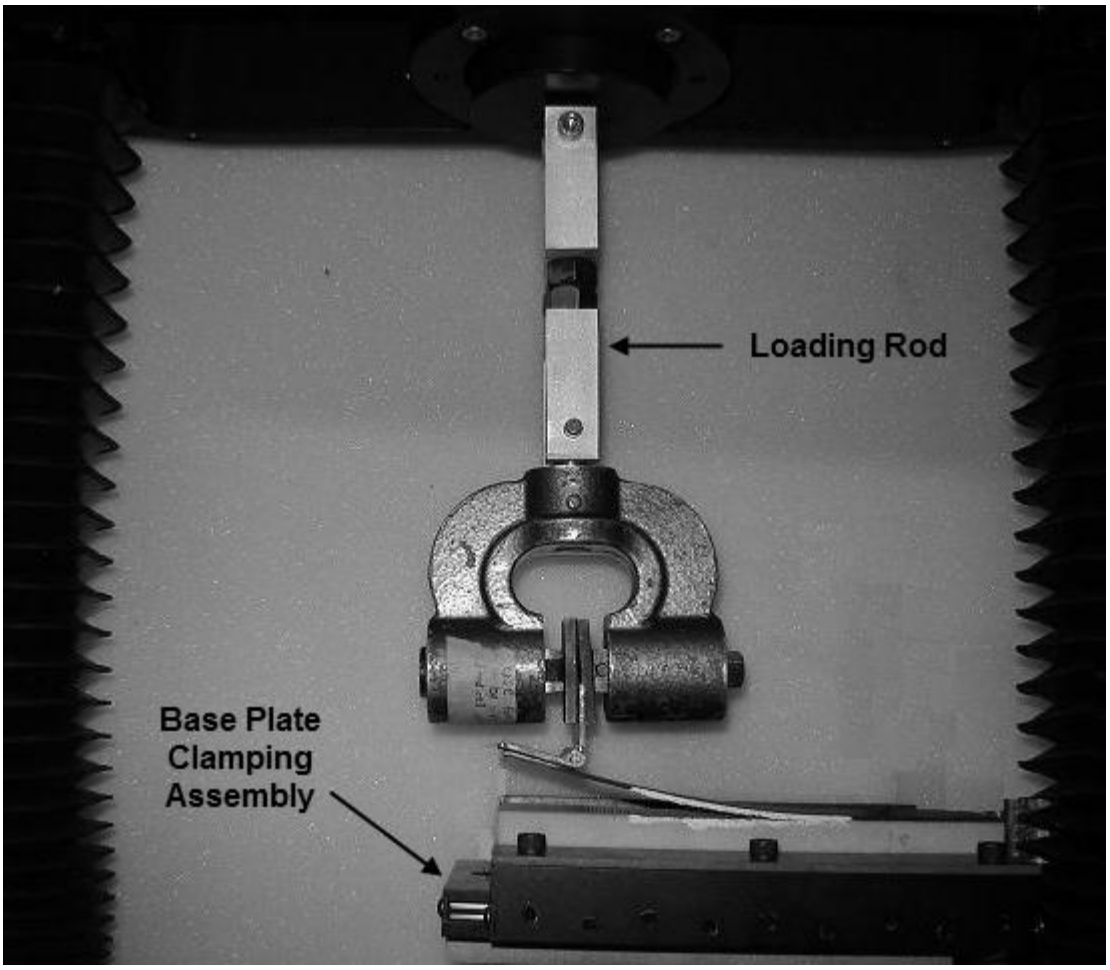

Figure B-2 Fixturing for SCB Testing

specimen grips attached, is less than 2 % of the opening displacement of the test specimen. If not, then the opening displacement shall be obtained from a properly calibrated external gage or transducer attached to the specimen. The displacement indicator shall indicate the crack opening displacement with an accuracy of within ±1 % of the indicated value once the delamination occurs.

7.3 *Load Versus Opening Displacement Record*—An *X-Y* plotter, or similar device, shall be used to make a permanent record during the test of load versus opening displacement at the point of load application. Alternatively, the data may be stored digitally and post-processed.

7.4 *Optical Microscope*—A travelling optical microscope with a magnification no greater than 70×, or an equivalent magnifying device, shall be positioned on one side of the specimen to observe the delamination front as it extends along one edge during the test. This device shall be capable of pinpointing the delamination front with an accuracy of at least ±0.5 mm (±0.02 in.). A mirror may be used to determine visually any discrepancy in delamination onset from one side of the specimen to the other. Other methods, such as crack length gages bonded to a specimen edge, may be used to monitor delamination length, provided their accuracy is as good as the optical microscope so that delamination length may be measured to the accuracy specified above.

7.5*Micrometers* – The micrometer(s) shall use a suitable size diameter ball interface on irregular surfaces such as the bag side of a laminate and a flat anvil interface on machined edges or very smooth tooled surfaces. The accuracy of the instruments shall be suitable for reading to within 1 % of the sample width, typically an accuracy of ±25 μm (0.001 in.) is desirable.

8. Sampling and Test Specimens

8.1 A nonadhesive insert shall be inserted between the core and one of the sandwich facings. If a film adhesive is being used to bond the facing to the core, the insert should be placed between the core and the film adhesive rather than the between the film adhesive and the facing. The film thickness shall be no greater than 13 μm (0.0005 in.). Specimens should not be precracked before testing. A polymer film is recommended for the insert to avoid problems with folding or crimping at the cut end of the insert, as has been observed in similar testing using aluminum foil inserts. For epoxy matrix composites cured at relatively low temperatures, 177°C (350°F) or less, a thin film made

of polytetrafluoroethylene (PTFE) is recommended. For composites with polyimide, bismaleimide, or thermoplastic matrices that are manufactured at relatively high temperatures, greater than 177°C (350°F), a thin polyimide film is recommended. For materials outside the scope of this test method, different film materials may be required. If a polyimide film is used, the film shall be painted or sprayed with a mold release agent before it is inserted in the laminate. (**Warning**—Mold release agents containing silicone may contaminate the panel. It is often helpful to coat the film at least once and then bake the film before placing the film on the composite. This will help to prevent silicone migration within the panel. Although precracking is not recommended, under certain prescribed circumstances (see 11.7.7) an alternate wedge precracking procedure may be used. Guidelines for generating a wedge precrack are given in Annex A3.)

8.2 *Specimen Dimensions* -- Minimum specimen dimensions for various types of core materials are as follows:

8.2.1 *Continuous Bonding Surfaces (for example, balsa wood, foams)* – The minimum width of the specimen shall be at least 50.8mm (2.0 in.) wide.

8.2.2 *Discontinuous Cellular Bonding Surfaces (for example, honeycomb)* – The required width of the specimen is dependent upon the cell size, to ensure a minimum number of cells are tested. A minimum specimen width of 50.8 mm (2.0 in.) is recommended and the largest practical specimen width for this test method is 76.2 cm (3.0 in.). These recommended widths are intended to provide approximately 6 cells minimum across the width of the specimen. Cores with cell sizes larger than 9 mm (0.375 in.) may require a smaller number of cells to be tested in the specimen.

8.2.3 Specimens shall be at least 178 mm (7 in.) long.

8.3 Panels shall be manufactured, and specimens cut from the panels, such that the insert length is approximately 50.8 mm (2.0 in.). This distance corresponds to an initial disbond length of approximately 25.4 mm (1.0 in.) plus the extra length required to bond the hinges or load blocks. The end of the insert should be accurately located and marked on the panel before cutting specimens.

8.4 The initial delamination length, measured from the load line to the end of the insert, shall normally be 25.4 mm (1.0 in.). However, alternative initial disbond lengths may be chosen.

8.5 *Sampling*—Test at least five specimens per test condition unless valid results can be gained through the use of fewer specimens, such as the case of a designed experiment. For statistically significant data, the procedures outlined in Practice E122 should be consulted. The method of sampling shall be reported.

8.6 *Load Introduction*:

8.6.1 The piano hinges or loading blocks shall be at least as wide as the specimen.

8.6.2 *Piano Hinges*—A piano hinge tab shall be bonded to the end of each specimen as shown in Fig. 1*a*. The hinge tabs shall be made of metal and shall be capable of sustaining the applied load without incurring damage.

8.6.3 *Loading Blocks*—The distance from the loading block pin to the center line of the top facing shall be as small as possible to minimize errors as a result of the applied moment arm.

8.6.4 The bonding surfaces of the loading blocks or hinges and the specimen shall be properly cleaned before bonding to ensure load transfer without debonding during the test. If debonding of the loading blocks or hinges occurs, the specimen should not be

reused if there is physical evidence that disbond growth initiated when the bond failed or if an increased compliance is observed upon reloading.

8.6.4.1 *Surface Preparations of the Specimen*—The bonding surface of the specimen may be lightly grit blasted or scrubbed with sandpaper, then wiped clean with a volatile solvent, such as acetone or methylethylketone (MEK), to remove any contamination.

8.6.4.2 *Surface Preparation of the Loading Hinge Tabs or Blocks*—The loading hinge tabs or blocks may be cleaned as in 8.6.4.1. If this procedure results in a bond failure between the specimen and the tabs, it may be necessary to apply a more sophisticated cleaning procedure based on degreasing and chemical etching. Consult Guide D2651 for the surface preparation procedure that is most appropriate for the particular metal used for the hinges or loading blocks.

8.6.5 Bonding of the loading hinges or blocks to the specimen shall be performed immediately after surface preparation. The material recommended for bonding is a room temperature cure adhesive. However, in some cases, a superglue, such as cyanoacrylate, has been found to be sufficient. The adhesive may benefit from a postcure if the specimens are dried after the loading hinges or blocks are mounted. Glass beads may need to be added to some adhesives, or other forms of bondline control may be needed to maintain a uniform bond thickness. The loading hinge or block shall be aligned parallel with the specimen and held in position with clamps while the adhesive cures.

8.6 *Labeling* – Label the test specimens so that they will be distinct from each other and traceable back to the panel of origin, and will neither influence the test nor be affected by it.

9. Calibration

9.1 The accuracy of all measuring equipment shall have certified calibrations that are current at the time of use of the equipment.

10. Conditioning

10.1 *Standard Conditioning Procedure*— Condition in accordance with Procedure C of Test Method D5229/D5229M unless a different environment is specified as part of the experiment. Store and test specimens at standard laboratory atmosphere of 23 ± 3°C (73 ± 5°F) and 50 ± 10 % relative humidity.

10.2 *Drying*—If interface fracture toughness data are desired for sandwiches in a dry condition, use Procedure D of Test Method D5229/D5229M.

11. Procedure

11.1 Measure the width of each specimen to the nearest 0.05 mm (0.002 in.) at the midpoint and at 25 mm (1 in.) from either end. The variation in thickness along the length of the specimen shall not exceed 0.1 mm (0.004 in.). The average values of the width and thickness measurements shall be recorded.

11.2 Coat both edges of the specimen just ahead of the insert with a thin layer of water-based typewriter correction fluid, or equivalent, to aid in visual detection of disbond onset. Mark the first 5 mm (0.2 in.) from the insert on either edge with thin vertical lines every 1 mm (0.04 in.). Mark the remaining 20 mm (0.8 in.) with thin vertical lines every 5 mm (0.2 in.). The disbond length is the sum of the distance from the loading line to the end of the insert (measured in the undeformed state) plus the increment of growth determined from the tick marks.

11.3 Connect to one end of the loading rod a wedge grip, if hinges are being used, or if load blocks are being used, a yoke compatible with the block. Connect the opposite end of the loading rod to the upper head of the test machine.

11.4 Mount the specimen on the base plate using the side clamps, making sure the load block or hinge on the specimen is aligned and centered with the loading rod.

11.5 As load is applied, measure the disbond length, *a*, on one side of the specimen. The initial disbond length, a_0, is the distance from the load line to the end of the insert. Do not try to locate the end of the insert by opening the specimen. If it is difficult to see the end of the insert on the specimen edge, or to locate the end of the insert from the original mark on the panel, try the following: (1) rub the edge of the specimen in the local area near the insert with a soft lead pencil and (2) polish the edge of the specimen. If none of the above methods are suitable, mark graduations on the specimen edge from the center of the loading pin. When the specimen is loaded, the length of the initial disbond may be determined from these graduation marks. When the disbond grows from the insert, take the first reading at the next whole 1-mm mark. Then, take readings for the next four 1-mm increments of disbond growth and subsequent 5-mm increments as specified above.

11.6 Set an optical microscope (see 7.4), or an equivalent magnifying device, in a position to observe the motion of the disbond front as it grows along one edge. This device shall be capable of pinpointing the disbond front with an accuracy of at least ±0.5 mm (±0.02 in.).

11.7 *Initial Loading*:

11.7.1 Load the specimen at a constant crosshead rate between 1 and 5 mm/min.

11.7.2 Record the load and the displacement values, continuously if possible. Record the position of the delamination with an accuracy of at least ±0.5 mm.

11.7.3 During loading, record the point on the load-displacement curve, or the load-displacement data values, at which the visual onset of disbond movement was observed on the edge of the specimen.

11.7.3.1 Record the load and displacement values at as many disbond length increments as possible in the first 5 mm, ideally every 1 mm. Subsequently, record these load and displacement data at every 5 mm, until the delamination crack has propagated at least 45 mm from the tip of the precrack, and again at every 1-mm increment of crack growth for the last 5 mm of disbond propagation, up to total disbond length of 50 mm beyond the tip of the precrack (Figure B-3).

11.7.4 Finally, unload the specimen at a constant crosshead rate of up to 25 mm/min.

11.7.5 Mark the positions of the tip of the delamination crack after unloading on both edges of the specimen. Note in the report if these positions differ by more than 2 mm.

11.7.6 Any permanent deformation of the specimen after unloading shall be noted in the report. Deviations of the disbond from the facing/core interface of the sandwich will

invalidate the test results and shall be noted in the report. A replacement specimen shall be tested.

11.8 *Visual Observation* —A visual initiation value for G_{Ic} should be recorded corresponding to the load and displacement for the first point at which the disbond is visually observed to grow from the insert on either edge using the microscope or mirror, or both, specified in 7.5.

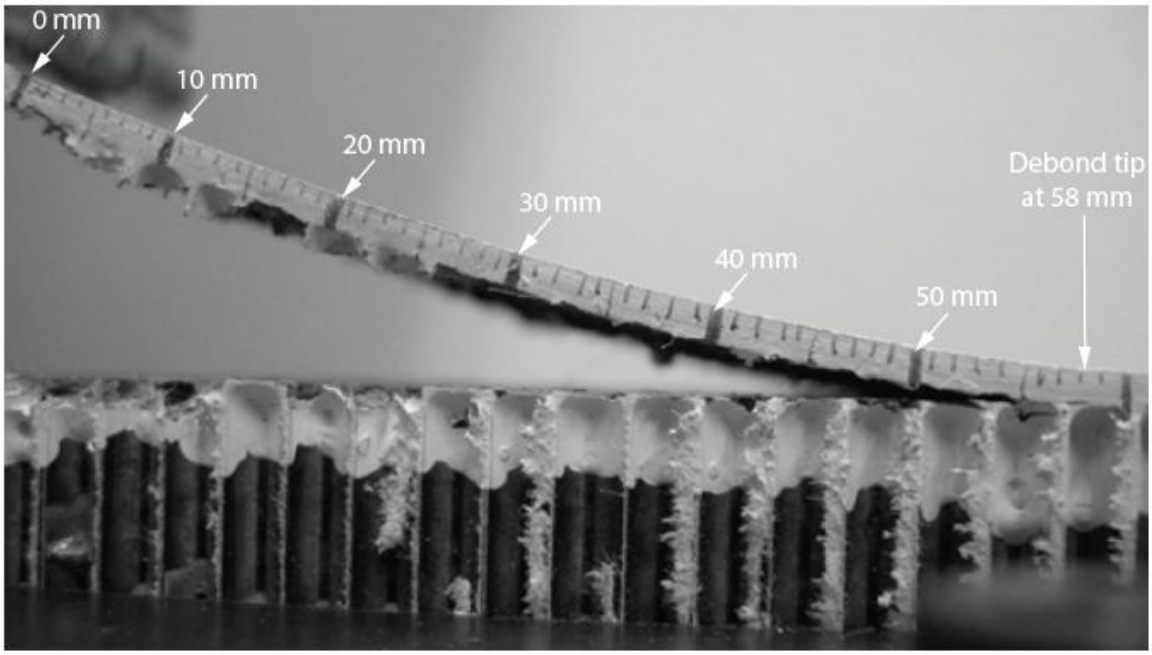

Figure B-3: Test coupon at the end of testing showing debond growth greater than 50 mm

12. Calculation

12.1 *Interlaminar Fracture Toughness Calculations* —The compliance calibration method (CC) is the data reduction method recommended for reducing data and calculating G_{Ic}.

12.1.1 *Compliance Calibration (CC) Method*— Generate a least squares plot of log (δ_i/P_i) versus log (a_i) using the visually observed delamination onset values and all the propagation values. Draw a straight line through the data that results in the best least-squares fit. Calculate the exponent n from the slope of this line according to $n = \Delta_y/\Delta_x$. Calculate the Mode I interlaminar fracture toughness as follows **(9)**:

$$G_I = \frac{nP\delta}{2ba} \qquad (9)$$

13. Report

13.1 A recommended data reporting sheet is shown in Annex A1. The report shall include the following (reporting of items beyond the control of a given testing laboratory, such as might occur with material details or panel fabrication parameters, shall be the responsibility of the requestor):

13.2 *Material*—Complete identification of the material tested; including prepreg and core manufacturer, material designation, manufacturing process, fiber volume fraction, and void content. Include the method used to determine fiber volume fraction and void content.

13.3 *Coupon Data*—Average width of each specimen, and thickness of insert.

13.4 *Test Procedure*—Type of load introduction (piano hinges or blocks) and dimensions, drying procedure, relative humidity, test temperature, and loading rate.

13.5 *Test Results*:

13.5.1 Load-displacement curves indicating load and displacement

13.5.2 Slope, n, of log (δ_i/P_i) versus log (a_i) plot for each specimen for which the compliance calibration (CC) method was used.

13.5.3 Report the number of specimens tested and the mean, standard deviation, and coefficient of variation (standard deviation divided by the mean) of quantities in.

14. Precision and Bias

14.3 *Bias*—No other test method exists for determining the Mode I interface fracture toughness of sandwich composites. Hence, no determination of the bias inherent in the SCB test is available.

15. Keywords

15.1 composite materials; sandwich, sandwich construction; core; facing; delamination; single cantilever beam; interface fracture toughness; Mode I

REFERENCES

1. "Standard Test Method for Mode I Interlaminar Fracture Toughness of Unidirectional Fiber-Reinforced Polymer Matrix Composites," ASTM D 5528, *Annual Book of ASTM Standards,* Vol. 15.03, ASTM International, West Conshohocken, PA, 2007.

2. Ratcliffe, J. G., Reeder, J. R., "Sizing a Single Cantilever Beam Specimen for Characterizing Facesheet/Core Peel Debonding in Sandwich Structure," *Journal of Composite Materials,* 2011 pp. 1-16.

3. "Standard Test Method for Flatwise Tensile Strength of Sandwich Constructions," ASTM C 297, *Annual Book of ASTM Standards*, Vol. 15.03, ASTM International, West Conshohocken, PA, 2007.

4. "Standard Test Method for Climbing Drum Peel for Adhesives," ASTM D 1781, *Annual Book of ASTM Standards,* Vol. 15.06, ASTM International, West Conshohocken, PA, 2011.

5. Weaver, C., "Evaluation of Mode I Fracture Mechanics Test Methods for Sandwich Composites," University of Utah, Salt Lake City, UT, 2009.

6. Kuromoto, B. K., "Development and Evaluation of a Mode I Fracture Mechanics Test Method for Sandwich Composites," University of Utah, Salt Lake City, UT, 2010.

7. General Plastics Manufacturing Company, LAST-A-FOAM FR6710 Rigid Polyurethane Foam Technical Data Sheet, *Technical Data Sheet Downloads*, [Online] 2011, [Cited: November 11, 2011.] http://www.generalplastics.com/knowledge-center/tech-data-downloads. FR-6710.

8. Hexcel Corporation**,** HexWeb HRH-10 Product Data, [Online] November 2006, [Cited: November 11, 2011.] http://www.hexcel.com/Resources/DataSheets/Honeycomb-Data-Sheets/HRH_10_us.pdf. HRH-10.

9. Li, X., Carlsson, L. A., "Elastic Foundation Analysis of Tilted Sandwich Debond (TSD) Specimen," *Journal of Sandwich Structures and Materials*, Vol. 2 , 2000 pp. 3-32.

10. Cytec, CYCOM 970 Epoxy Resin, *Cytec Engineered Materials.* [Online] August 10, 2001, [Cited: November 11, 2011,] https://www.cytec.com/engineered-materials/products/Datasheets/CYCOM%20970.pdf. CYCOM 970.

11. Momentive, Epoxy Resins, Curing Agents & Modifiers. *Momentiv,.* [Online] Momentive Specialty Chemical Company, 2010, [Cited: November 11, 2011] http://ww2.momentive.com/ProductFamily/epoxy_intermediates.aspx?id=225.

12. Davidson, B.D., Schapery, R. A., "Effect of Finite Width on Deflection and Energy Release Rate of an Orthotropic Double Cantilever Specimen," *Journal of Composite Materials*, Vol. 22, 1988.

13. Stanley, L. E., "Development and Evaluation of Stitched Sandwich Panels," University of Utah, Salt Lake City, UT, 2001.

14. Prasad, S., Carlsson, L. A., "Debonding and Crack Kinking in Foam Core Sandwich Beams – I. Analysis of Fracture Specimens," *Engineering Fracture Mechanics*, Vol. 47, 1994.

15. Prasad, S., Carlsson, L. A., "Debonding and Crack Kinking in Foam Core Sandwich Beams – II. Experimental Investigation," *Engineering Fracture Mechanics*, Vol. 47, 1994.

16. Ratcliffe J. G., Cantwell, W. J., "Center Notch Flexure Sandwich Geometry for Characterizing Skin-Core Adhesion in Thin-Skinned Sandwich Structures," *Journal of Reinforced Plastics and Composites*, Vol. 20, 2001.

17. Gates, T. S., Herring, H. M., "Facesheet Push-off Tests to Determine Composite Sandwich Toughness at Cryogenic Temperatures," *American Institute of Aeronautics & Astronautics*, Seattle, WA, 2001.

18. Williams, J. G., " The Fracture Mechanics of Delamination Tests," *Journal of Strain Analysis*, Vol. 24, 1989.

19. Broek, D., *Elementary Engineering Fracture Mechanics*, Martinus Nijhoff Publishers, Dordrecht, 1986.

20. Rybicki, E. F., Kannien, M. F., "A Finite Element Calculation of Stress Intensity Factors by a Modified Crack-Closure Integral," *Engineering Fracture Mechanics*, Vol. 9, 1977.

21. Gent, A. N., Hamed, G. R., "Peel Mechanics of Adhesive Joints," *Polymer Engineering and Science*, Vol. 17, 1977.

22. Kinloch, A. J., Lau, C. C., Williams, J. G., "The Peeling of Flexible Laminates," *International Journal of Fracture*, Vol. 66, 1994